

UNIVERSITÀ DEGLI STUDI DI NAPOLI FEDERICO II

SCUOLA POLITECNICA E DELLE SCIENZE DI BASE

DIPARTIMENTO DI INGEGNERIA CHIMICA, DEI MATERIALI E DELLA PRODUZIONE INDUSTRIALE



Ph.D. in Chemical Engineering

(XXVI Cycle)

**COMBUSTION INDUCED RAPID PHASE
TRANSITION OF CO/H₂/O₂/N₂/CO₂ MIXTURES**

Scientific committee

Prof. Gennaro Russo

Prof. Almerinda Di Benedetto

Prof. Martino Di Serio

Dott. Ernesto Salzano

Candidate

Ing. Anna Basco

INDEX

1. INTRODUCTION	3
2. STATE OF ART.....	8
2.1. Syngas combustion kinetic	8
2.2. Explosion modes: deflagration, detonation, deflagration to detonation transition, heat explosion and combustion-induced rapid phase transition of oxygen-enriched fuel mixtures	13
3. AIM OF THE WORK	25
4. METHODS	27
4.1. Experimental	27
4.2. Model	33
4.3. Thermochemical analysis	34
5. RESULTS	38
5.1. Explosive behavior of H ₂ /CO/O ₂ /N ₂ /CO ₂ mixture	38
5.1.1. Effect of E, φ and H ₂ /CO ratio	39
5.1.2. Laminar burning velocity	43
5.1.3. Effect of CO ₂	45
5.1.4. Correlation for laminar burning velocity.....	48
5.1.5. Anomalous behavior in syngas oxy-combustion explosions.....	51
5.2. Explosive behavior of H ₂ /CO/O ₂ /N ₂ mixtures.....	53
5.2.1. Explosion of CO/O ₂ /N ₂ mixtures: Effect of oxygen-air enrichment factor... 55	
5.2.2. Effect of H ₂ addition.....	56
5.2.3. Enhancement of reactivity due to H ₂ presence	57
5.3. Theoretical prediction of c-RPT occurrence.....	60
5.3.1. Analysis of literature data.....	68

6. CONCLUSIONS	71
7. REFERENCES	74

1. INTRODUCTION

Many processes of the chemical industry are facing increasing pressure to reduce fuel, operating costs, emissions and to improve quality, flexibility and capacity. The use of pure oxygen or oxygen-enriched air is an excellent way to achieve these results. Processes such as oxidation, fermentation, combustion and wastewater treatment can be improved by the use of oxygen especially for the increment of capacity which derives. Furthermore, limiting the amount of nitrogen in the process permits the use of smaller equipments. The overall flow is lower than that of an air-based process, thus minimizing pressure drops and reducing operating costs [Hendershot et al. 2010]. Table 1 lists major petrochemical processes that utilize air, pure oxygen, oxygen enriched air or other oxidants. The use of oxygen can often be justified by improved reaction rates, selectivity and yields.

Table 1. *Petrochemical processes which employ air, oxygen, oxygen enriched air or chlorine [Hendershot et al. 2010].*

Chemical	Manufacturing process options
Ethylene oxide	Oxygen, air
Propylene oxide	Oxygen, air, chlorine
Acetaldehyde	Oxygen, air
Vinyl chloride	Oxygen, air, chlorine
Vinyl acetate	Oxygen
Caprolactam	Oxygen, air
Terephthalic acid	Air, oxygen enriched air
Maleic anhydride	Air, oxygen enriched air
Acrylonitrile	Air, oxygen enriched air
Phenol	Air, oxygen enriched air
Isophthalic acid	Air, oxygen enriched air

The production of ethylene oxide from ethylene is one of these processes: because nitrogen does not need to be purged from the reactor, which is an operation that implies several steps, and because the use of pure oxygen allows the reaction to occur at optimum kinetic conditions, the process can be run in a single stage.

Another interesting process which uses highly oxygen-enriched air is the “oxy-combustion”. This technology is used in several applications, including glass manufacturing, ferrous and nonferrous metal processing, waste incineration, sulfur recovery, fluid catalytic cracking, power generation and many others.

Oxygen enriched combustion can be accomplished with low-level, medium-level or high-level enrichment. Low-level enrichment is defined as a mole fraction of oxygen in the oxidant stream between 21% and 28% and represents the simplest and lowest-cost implementation since oxygen can be added directly to the main air stream ducts and can be used the existing burners. Higher levels of oxygen concentration require specialized burners and equipments, but they also provide higher levels of benefits.

Nowadays the interest towards oxy-fuel combustion for power generation is increasing because it is an important step towards zero-emission combustion technology. Indeed:

- i) the reduced amount of nitrogen reduces the overall NO_x emissions;
- ii) the higher reactivity of oxygen allows the use of lean and more in general low reactivity fuel mixtures, thus decreasing the flame temperature (i.e. lower equipment cost and further decrease of NO_x emissions);
- iii) the exhausted gas stream contains mainly carbon dioxide and water vapor, thus favoring any subsequent CO₂ sequestration [Dennis, 2006; Lieuwen et al., 2010] (Figure 1).

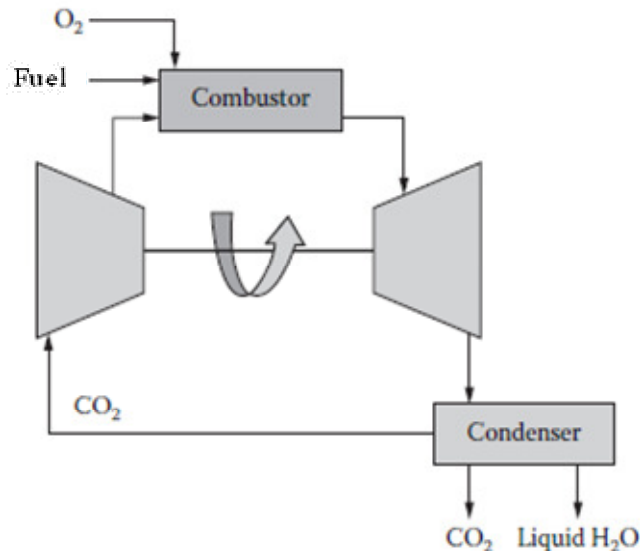


Figure 1. Scheme of a typical oxy-fuel power cycle for CO_2 sequestration [Lieuwen et al. 2010].

On the other hand, despite the environmental and sustainability advantages of oxy-combustion, Lieuwen et al. (2010) have stated that the use of highly enriched O_2 oxidizer implies substantial cost penalty and potential corrosion concerns. These issues have forced process designer towards the adoption of near stoichiometric conditions or even more diluted mixtures in order to reduce oxygen demand. The use of oxygen-enriched air poses however severe safety issues, because pure oxygen enlarges the flammability range with respect to air, as showed in Table 2 [Cohen, 1992].

Table 2. Flammability limits of several fuels in air and O_2 [Cohen, 1992]

Gas	Limits in air, % _{v/v}		Limits in O_2 , % _{v/v}	
	Lower	Upper	Lower	Upper
Hydrogen	4.0	75.0	4.0	94.0
Carbon monoxide	12.5	74.0	15.5	94.0
Methane	5.3	14.0	5.1	61.0
Ethane	3.0	12.5	3.0	66.0
Propane	2.2	9.5	2.3	55.0
Butane	1.9	8.5	1.8	49.0

Also, the burning velocity is modified by the increasing of oxygen concentration in the oxidizer. Figure 2 shows the effect of oxygen enhancement on burning velocity for $\text{CH}_4/\text{O}_2/\text{N}_2$ mixtures [Lewis & Von Elbe, 1961].

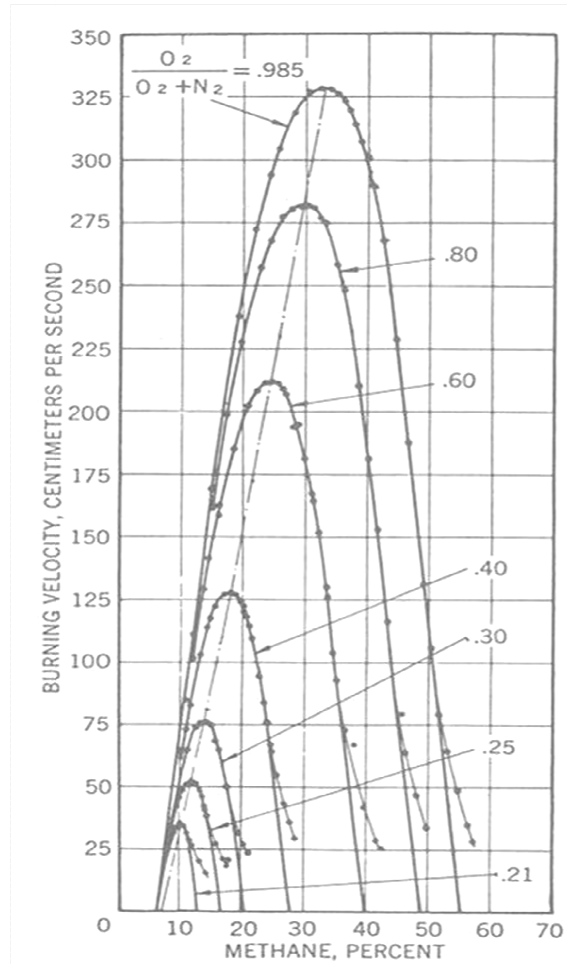


Figure 2. Enhancement of laminar burning velocity with oxygen concentration for $\text{CH}_4/\text{O}_2/\text{N}_2$ mixtures [Lewis & Von Elbe, 1961].

Once fixed the percentage of CH_4 in the mixture, the burning velocity significantly increase as O_2 content in the oxidizer increases. These effects are even more hazardous when hydrogen is present in the fuel mixture because its presence makes the mixture highly reactive, thus enhancing the risk of explosion, in particular, literature results show that the risk for deflagration to detonation transition, heat explosion or combustion induced rapid phase transition is significantly enhanced [Lee, 2008; Safekinex, 2009; Di Benedetto

et al., 2009]. On the other hand, the dilution with CO₂ results in substantial decreases of either the laminar burning velocity, or the flammability range and the flame temperature by thermal and kinetic effects [Arpenteiner et al., 2001].

The ability of oxy-combustion to operate with low reactivity fuels is largely advantageous for the general aims of energetic sustainability. In this framework, the use of syngas (a mixture composed of H₂, CO, CO₂, H₂O, CH₄ and other minor components) derived from biomass gasification, pyrolysis, or waste gases is greatly increasing due to the valorization of those secondary materials for power generation and more in general towards zero-emission combustion technology.

This Ph.D activity has been devoted to the study of the explosive behavior of syngas combustion in oxygen enriched air, with specific attention to the evaluation of the main factors (fuel composition, diluents content, oxygen enrichment), able to trigger anomalous explosive behaviors.

2. STATE OF ART

Literature review has highlighted that most of scientific works on oxy-combustion deals generally with the explosion behavior of pure hydrocarbons, whereas very few analyses have been devoted to the study of the explosion of syngas in oxygen-enriched air. As a consequence, an extensive study of syngas oxy-combustion is mandatory, starting from the state of the art of the combustion kinetic of syngas with both air and oxygen and of the main explosion phenomena which may occur in such fuel-oxidant mixtures.

2.1. Syngas combustion kinetic

Lieuwen et al. (2010) state that technical development are hindered by the lack of fundamental data on burning velocity for diluted syngas oxy-combustion, even if several experimental and numerical studies are available in the literature when using air as oxidant. A review of the influence of H_2/CO ratio, initial pressure and preheat temperature, dilution and flame stretch on the laminar flame speed of syngas fuel mixtures in air is largely analyzed in Lieuwen et al. (2010).

When a typical hydrocarbon fuel reacts with air, the kinetic of the combustion reaction is ruled by the generation and propagation of radical species. As it regards CO combustion, in the absence of hydrogen containing species, the reactions involving O radical and CO are very slow. Indeed it is extremely difficult to ignite and to have a flame propagation in such mixtures. As H_2 molecules or other species hydrogen containing (as H_2O for instance) are added to CO, the reaction rate rises considerably because hydrogen radicals diffuse very rapidly through propagation reactions, which involve H atoms.

The kinetic models for CO/H₂/O₂ combustion reaction are fundamental for the understanding of combustion chemistry. One of the first validated kinetic study was that of Yetter et al. (1991), which elaborated a reaction scheme for syngas/air combustion system and developed a detailed kinetic mechanism, which has been confirmed and further developed in several following studies. In particular, Davis et al. (2005) developed a kinetic scheme consisting of 14 species and 30 reactions modifying the enthalpy of formation of the OH radical and the rate coefficient of the third-body reaction:



A study by Bouvet et al. (2011) carried out syngas laminar flame speed measurements at atmospheric pressure and ambient temperature by using spherically expanding flames. Mixture compositions ranging from H₂/CO = 5%/95% to H₂/CO = 50%/50% and equivalence ratios from 0.4 to 5.0 have been investigated. Flame speed measurements for all investigated syngas/air mixtures have been compared with the predictions calculated with the Li et al. (2007) mechanism. It can be observed that calculations generally over-predict the experimental values.. The agreement is good for both 5/95% and 10/90% H₂/CO mixtures for the very rich branch but measurements are higher than predictions for both 25/75% and 50/50% H₂/CO cases.

Recently, due to the high interest in gas turbine syngas combustion, several experiments have been executed at temperature and pressure higher than atmospheric values [Burke et al., 2007; Mittal et al., 2007; Natarajan et al., 2007; Petersen et al., 2007; Sun et al., 2007; Walton et al., 2007].

Natarajan et al. (2007) evaluated, either numerically or experimentally, the laminar flame speed of singas/air mixture at different compositions and values of initial pressure and

temperature, thus validating the mechanism formulated by Davis, in particular for high hydrogen content mixtures.

Burke et al. (2007) have measured syngas/air laminar flame speeds in cylindrical test chamber with outwardly propagating spherical flames, at constant pressure. The results are reported for H₂/CO/CO₂ mixtures by varying in equivalence ratio from 0.6 to 4.0, pressure from 1 to 20 bar, and CO₂ dilution from 0% to 25%. The experimental measurements were compared with experiments performed by McLean et al. (1994), Sun et al. (2007), and Hassan et al. (1997) and with the numerical results obtained by using the kinetic mechanisms of Li et al. (2007), Davis et al. (2005), and Sun et al (2007). These three mechanisms yield similar results, but Sun et al. predict slightly higher flame speeds than Li et al., which predict slightly higher flame speeds for low CO₂ concentrations and a slightly stronger adverse dependence of CO₂ concentration on the flame speed than Davis et al.,(2005).

Mittal et al. (2007) conducted experimental and numerical studies to evaluate the mechanism for the combustion of CO/H₂ mixtures in air at high pressures in the range of 15÷50 bar and temperatures in the range of from 950÷1100 K. Experiments were performed in a rapid compression machine. Autoignition delays were measured for stoichiometric compositions of CO/H₂ containing an amount of CO between 0% and 80% in the fuel mixture. The experimental results showed a monotonic increase of time delay as the content of CO in the fuel mixture was increased. By contrast, numerical simulations for the same mixtures based on the kinetic model derived by Davis et al., (2005) displayed a qualitative discrepancy with experimental values. The discrepancy is attributed to the value of the reaction rate constant recommended by Baulch et al. (1973) for the HO₂ + CO reaction, at T=1000 K, which could be up to a factor of 10 too high. Lowering this rate the qualitative anomaly between experiment and numerical prediction can be corrected

An important aspect to evaluate is the role of diluents during the process of syngas combustion. A study by Ding et al. (2011) investigate the extinction limits and emission formations of dry syngas (50% H₂ - 50% CO), moist syngas (40% H₂ - 40% CO - 20% H₂O), and impure syngas containing 5% CH₄ at two different pressures (1 bar and 5 bar, respectively). A counter-flow flame configuration was numerically investigated in order to understand flame extinction and emission characteristics at the lean-premixed combustion conditions, by varying inert content of N₂, CO₂ and H₂O at different pressures and syngas compositions. The OPPDIF model in CHEMKIN (Reaction Design®) along with the Davis mechanism have been utilized for the modeling of the oxidation of H₂/CO, whereas the GRIMech 3.0 mechanism has been utilized for oxidation of H₂/CO/CH₄. By increasing syngas composition and inert concentration, numerical simulation showed that: i) CO₂ diluted mixtures has the same extinction limit as moist or dry syngas, but show higher extinction temperature; ii) the presence of H₂O in the fuel mixture decreases the extinction limit of N₂ diluted flame but increases the flame extinction temperature; iii) the presence of CH₄ (impure syngas) determines larger flame extinction limit but has no effect on flame temperature in CO₂ diluted flame; iv) for diluted moist syngas, extinction limit is enlarged at higher pressure; v) higher CO concentration leads to higher NO emission.

Prathap et al. (2008) investigated the effect of dilution with nitrogen on the laminar burning velocity and flame stability of syngas fuel (50% H₂ – 50% CO) – air mixtures. The syngas fuel composition considered included an amount of N₂ from 0% to 60%. Spherically expanding flames were generated by centrally igniting homogeneous fuel–air gas mixtures in a 40-L cylindrical combustion chamber fitted with optical windows. Experiments were conducted at atmospheric conditions and equivalence ratios ranging from 0.6 to 3.5. All the measurements were compared with the numerical predictions obtained by using RUN-1DL and PREMIX coupled with Davis chemical kinetic scheme.

The effect of dilution with nitrogen resulted in: i) a decrease in the laminar burning velocity by reducing the thermal diffusivity and flame temperature of the mixture. iii) a shift in occurrence of peak laminar burning velocity from $\phi = 2.0$ for 0% N₂ dilution to $\phi = 1.4$ for 60% N₂ dilution, iv) an augmentation of the coupled effect of flame stretch and preferential diffusion on laminar burning velocity, and v) a shift in the equivalence ratio for transition from stable to unstable flames from $\phi = 0.6$ for 0% N₂ dilution to $\phi = 1.0$ for 60% N₂ dilution.

A study by Richards et al. (2005) have showed how the oxidation rate of CO in the syngas/air system is reduced by the presence of CO₂ in the reacting mixture, hence determining longer residence time for the complete combustion. This effect can be attributed to either thermal effects, due to the lower adiabatic temperature or the slower laminar flame speed due to the kinetic role of CO₂.

In this framework, a study by Di Benedetto et al. (2009) have evaluated the effect of CO₂ addition to CH₄/O₂/N₂ and H₂/O₂/N₂ at stoichiometric conditions and at different levels of oxygen-enrichment. The presence of CO₂ has been shown to affect significantly the laminar burning velocity up to flame extinction. The simulations have shown that the main role of CO₂ is to induce changes in the heat capacity of the mixture, hence lowering the flame temperature. The presence of CO₂ has been found to play also a kinetic role.

2.2. Explosion modes: deflagration, detonation, deflagration to detonation transition, heat explosion and combustion-induced rapid phase transition of oxygen-enriched fuel mixtures

When igniting a gaseous fuel premixed with air or oxygen, a self-sustained reaction (combustion) wave is observed. This phenomenon is defined as deflagration and is typically characterized by low flame speed. If occurring in confined or partially confined system, the chemical energy stored in the fuel is converted into the internal energy of the gaseous combustion products. As a consequence, the temperature is raised and expand against the walls thus increasing the internal pressure. In the case of isobaric expansion, as in the open, the same expansion may produce pressure waves which travel from the explosion source in the atmosphere.

Under appropriate conditions, a flame can continuously accelerate and undergo transition to a detonation wave (DDT). The main physical differences between detonation and deflagration mode for a combustion reaction that occurs in the gas phase in the open are shown in Figure 3 [Crowl & Louvar, 2002]. In the deflagration mode, the reaction front propagates at a speed less than the speed of sound. The pressure front moves at the speed of sound in the unreacted gas and moves away from the reaction front. In the case of detonation, the reaction front moves at a speed greater or equal than the speed of sound, and the shock front is found at short distance in front of the reaction front.

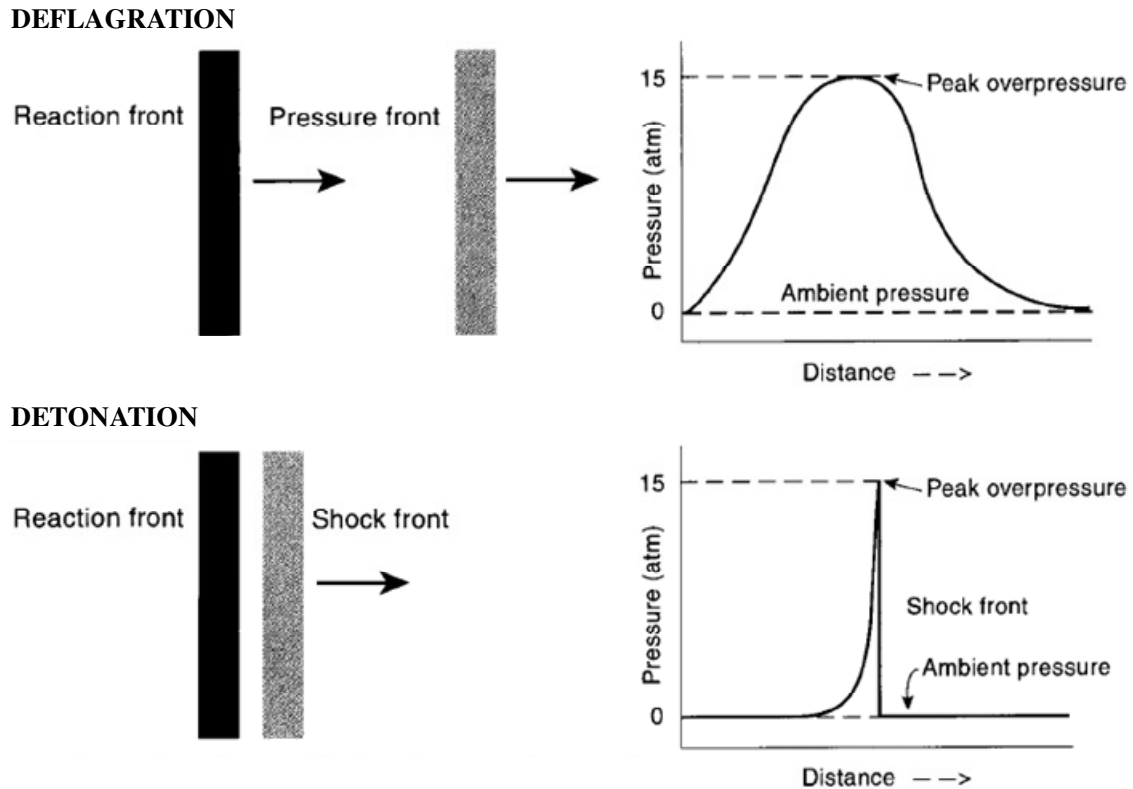


Figure 3. The reaction wave and the pressure (or shock) for the deflagration and detonation phenomena [Crowl & Louvar, 2002].

The pressure fronts produced by detonations and deflagrations are markedly different. A detonation produces a shock front, with an abrupt pressure rise, a maximum pressure of greater than 10 bar, and total duration of typically less than 1 ms. The pressure front resulting from a deflagration is characteristically wide (many milliseconds in duration), flat (without an abrupt shock front), and with a maximum pressure much lower than the maximum pressure for a detonation (typically 1 or 2 bar). The behaviors of the reaction and pressure fronts differ from those shown in Figure 3 depending on the local geometry constraining the fronts. Different behavior occurs if the fronts propagate in a closed vessel, a pipeline, or through a congested process unit.

The mechanism by which a deflagration transforms into a detonation remains one of the most interesting unresolved problems in combustion theory because of the numerous parameters which need to take into account. Transition from deflagration to detonation

(DDT) can be observed in a wide variety of situations, including flame propagation in smooth tubes or channels, flame acceleration caused by repeated obstacles, and jet ignition. The processes leading to detonation can be classified into two categories: i) detonation initiation resulting from shock reflection or shock focusing, i.e. a direct initiation process where the shock strength is sufficient to auto-ignite the gas and promote detonation; ii) transition to detonation caused by instabilities near the flame front or caused by flame interactions with a shock wave, walls or obstructed channels.

The first mechanism is much more probable when the shock interacts with a corner or a concave wall that produces shock focusing. It has also been found to be very efficient in promoting detonation for relatively slow flames.

Lee (2008) have proposed a theory on the development of detonation waves based on the so-called SWACER mechanism (Shock Wave Amplification by Coherent Energy Release). The mechanism proposed is based on the formation of an induction time gradient associated with temperature and concentration gradients that can produce a spatial time sequence of energy release. This sequence can then produce a compression wave that is gradually amplified into a strong shock wave that can auto-ignite the mixture and produce DDT.

Transition from high speed flame to detonation in tubes was studied in an extensive series of experiments with the aim of establishing quantitative limiting criteria for the onset of transition.

A necessary condition for transition to detonation is that the minimum transverse tube dimension, corresponding to the tube diameter d , must be sufficiently large to accommodate at least one transverse cell width characteristic of the mixture in the tube. That is, the quantitative criterion for transition is that $\lambda/d < 1$. Once established, the detonation wave in the tube within the obstacle field is observed to propagate at a steady

velocity. This criterion was specifically treated by Dupré et al. (1990) who presented a comprehensive analysis of detonation limits and monitored the propagation of established detonations in fuel-air mixtures through a series of pipes of decreasing diameter until the detonation was observed to fail. Hence, critical pipe diameters were determined for the DDT occurrence. These data, obtained as a function of fuel type and equivalence ratio, were then compared to detonation cell sizes previously measured or defined, as that of Moen et al. (1982), who established the $\lambda = 1.7 D$ condition for DDT. Eventually, Dupré et al. (1990) concluded that detonations could not propagate if the detonation cell width λ of any fuel-oxidant mixture was greater than the pipe diameter D . This condition was considered a realistic limit criterion because of uncertainties in detonation cell structure near the limit.

Akbar et al. (1997) reported experimental values of cell width λ for $\text{CH}_4/\text{O}_2/\text{N}_2$ mixture as function of enrichment factor E . These results are reported in Figure 4.

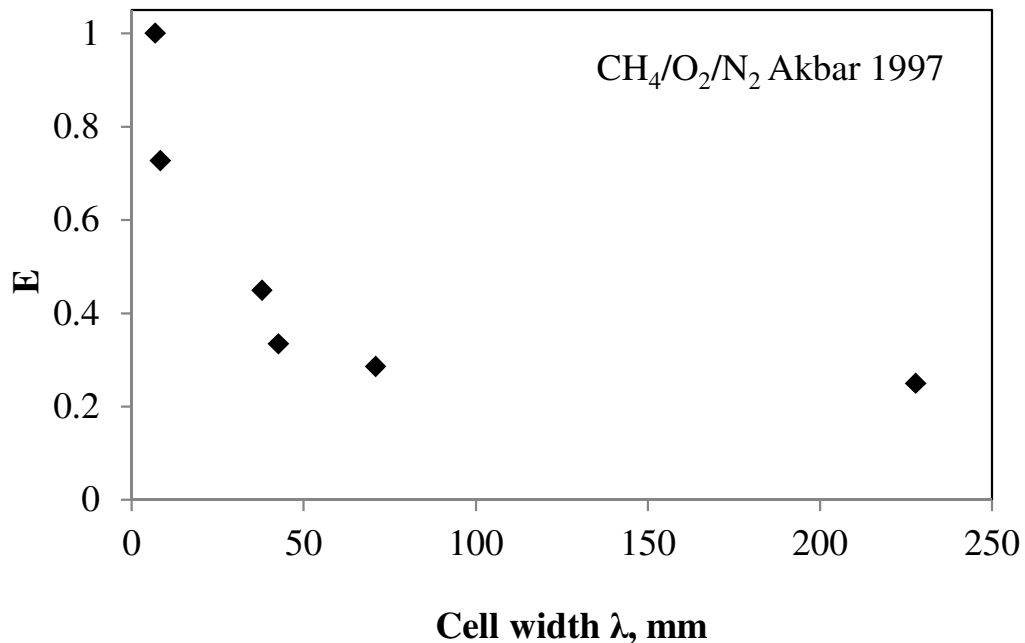


Figure 4: Characteristic cell width λ for $\text{CH}_4/\text{O}_2/\text{N}_2$ mixture varying enrichment factor E as given by Akbar (1997).

According to the results of Akbar, a CH₄/O₂/N₂ mixture with E = 0.3 can detonate in a tube if $\lambda = D = 70$ mm. The use of oxygen as oxidant rather than air makes deflagration to detonation transition (DDT) more likely. Furthermore, as for deflagration, detonation limits may be also affected, as clearly observed in Table 3, which reports detonation limit both in air and oxygen for several gases [Glassman & Yetter, 2008; Michels et al. 1970].

A study by Thomas (2009) shows the experimental pressure histories in various ethylene–oxygen compositions tested a 1.48 m long, 7 mm diameter tube at initial pressure and temperature of 1 bar and 293 K respectively (Figure 5). As the oxygen concentration increase from 40%_{v/v} to 48%_{v/v} the flame drastically accelerate and the detonation occurs.

Table 3. *detonation limits in oxygen and air [Glassman & Yetter, 2008; Michels et al., 1970]*

Gas	Lean limit, % _{v/v}		Rich limit % _{v/v}	
	Air	O ₂	Air	O ₂
H ₂	18.30	15.0	59.70	90.0
CH ₄	5.70	4.50	14.0	55.8
C ₂ H ₆	2.87	3.6	12.2	46.4
C ₃ H ₈	2.57	2.50	7.37	42.5
nC ₄ H ₁₀	1.98	2.05	6.18	38.0
nC ₈ H ₁₈	1.45	1.55	2.85	17.3
C ₂ H ₄	3.32	4.10	14.7	60.0
C ₃ H ₆	3.55	2.50	10.4	50.0
C ₂ H ₂	4.20	2.90	50.0	88.8

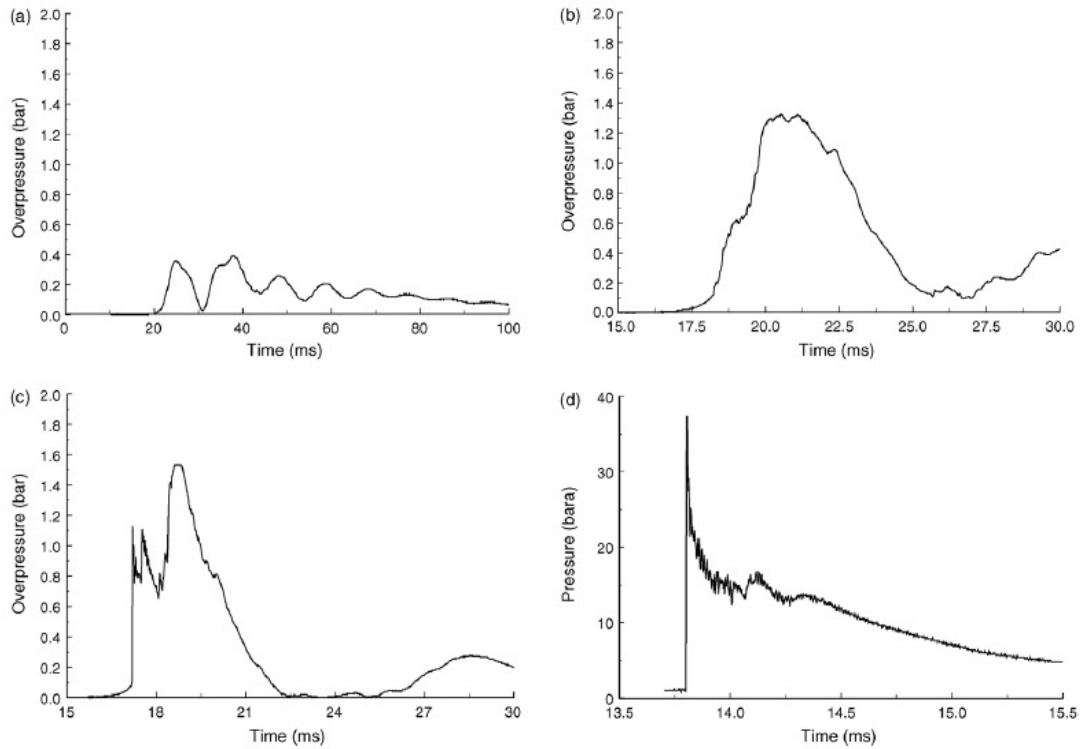


Figure 5. Representative pressure histories in various ethylene–oxygen compositions in a 1.48 m long 7 mm diameter tube. Pressure gauge at 1.28 m from spark source. Initial pressure 1 bar. Initial temperature 293 K. Oxygen concentration (a) 40% v/v, (b) 43% v/v, (c) 46% v/v and (d) 48% v/v. [Thomas, 2009]

Several fuel-air mixtures over a broad range of equivalence ratios at atmospheric initial condition were also studied by the same author. The results show that transition to detonation in tubes invariably occurs from a minimum level of flame speed corresponding roughly to the speed of sound of the combustion products. Since the flame speed in a tube is directly coupled to the flow field that it generates ahead of itself, this minimum flame velocity requirement implies that an adequate intensity of turbulent shear mixing is required to form the required explosive pocket of gas inherent in the genesis of detonation. Recently, BASF researchers (Safekinx, 2009), have tested the explosion behaviour of $\text{CH}_4/\text{O}_2/\text{N}_2$ mixtures with different compositions in a spherical vessel ($D = 340$ mm) at initial condition of temperature and pressure of 273K, 1 bar and 5 bar.

The pressure histories were recorded by piezoelectric pressure sensors with 500 kHz and sampling frequencies of up to 100 kSample/s. They found three explosion modes: deflagration, detonation and heat explosion as reported in the triangular diagrams of Figure 6.

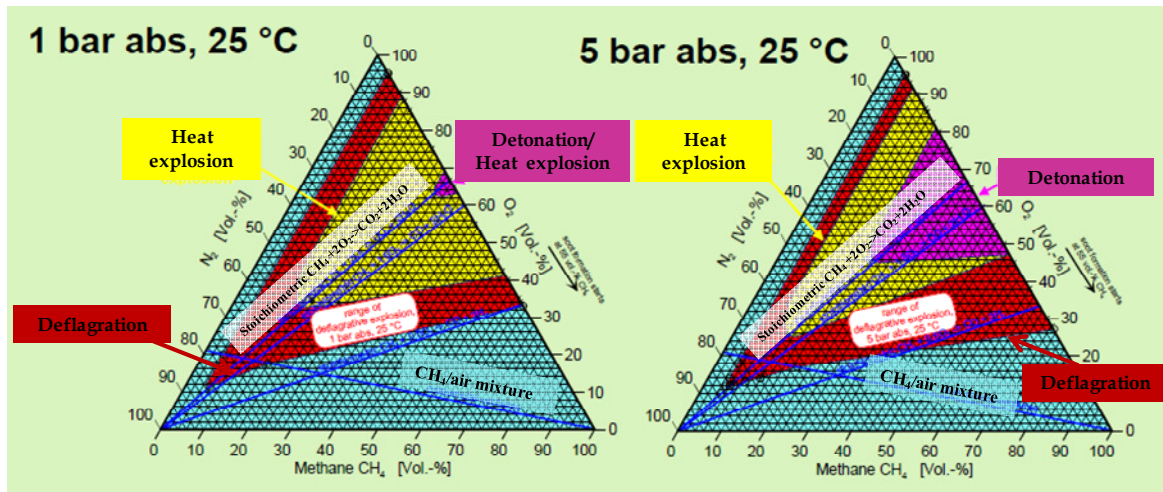


Figure 6. Triangular diagrams for $\text{CH}_4/\text{O}_2/\text{N}_2$ mixtures exploding in 20L sphere. [FP7 SAFEKINEX project, 2009]

To understand what really happens during heat explosion, in Figure 7 the pressure histories for three $\text{CH}_4/\text{O}_2/\text{N}_2$ compositions are reported. The pressure-time diagram at Figure 7a shows the typical story of deflagration combustion in closed vessel, with a maximum pressure (close to adiabatic pressure) and subsequent pressure decay due to heat losses towards vessel walls. The diagram of Figure 7c plots the a pressure time history typical of detonation, with a pressure peak which largely overcomes the adiabatic value. The plot reported in Figure 7b shows an explosive behavior which is significantly different from that of a detonation or a deflagration. The pressure time history measured during heat explosion exhibits an oscillating behavior and also an over-adiabatic peak. They recognized this explosion mode as different by DDT, and named it “heat explosion”: immediate temperature and pressure rise of un-reacted gases when heated by adiabatic

compression. The same researcher also affirmed that even if this anomalous behavior has been highlighted through experimental tests, the governing mechanisms of the heat explosion are not completely understood.

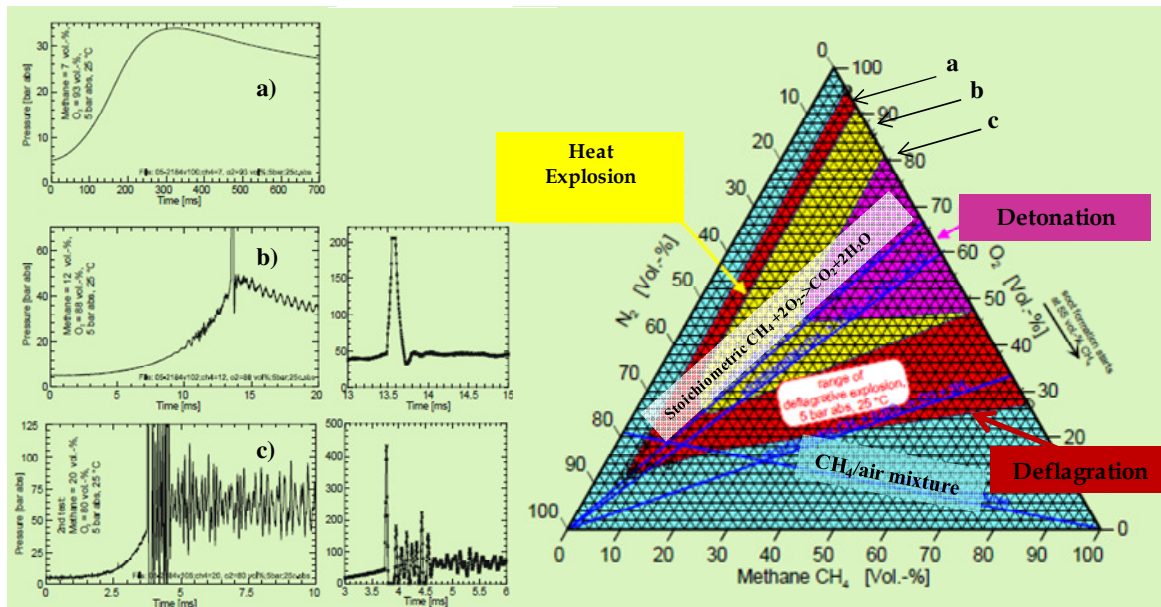


Figure 7. Pressure histories for CH_4/O_2 mixtures. [Safekinx, 2009]

Di Benedetto et al. (2011) found in oxygen-enriched methane-air mixtures a similar behavior during explosions in closed vessel, which exhibited oscillating pressure histories and peak pressure much higher than the thermodynamic. The plot of Figures 8 shows the pressure time history for the explosion of a mixture of $CH_4/O_2/N_2$ (molar composition: 16.7%, 33.3%, 50%) in a closed vessel of 5L volume. It is possible to distinguish three different phases which characterize the explosive behavior. A first phase in which the pressure history is typical of a deflagration in closed vessel. The adiabatic pressure is, in fact, achieved 0.0075 s after ignition which is the time required by the laminar flame to propagate along the entire length of the vessel. At this time, the combustion reaction is completed. After this time, the pressure starts decreasing due to the effect of heat losses.

During phase II the pressure signal starts to oscillate and the oscillation amplitude increases with time up to the over-adiabatic peak. It is worth noting that this peak appears when the combustion reaction has come to an end. In the last phase (III), the pressure trend is characterized by a gradual decay due to heat losses towards vessel walls.

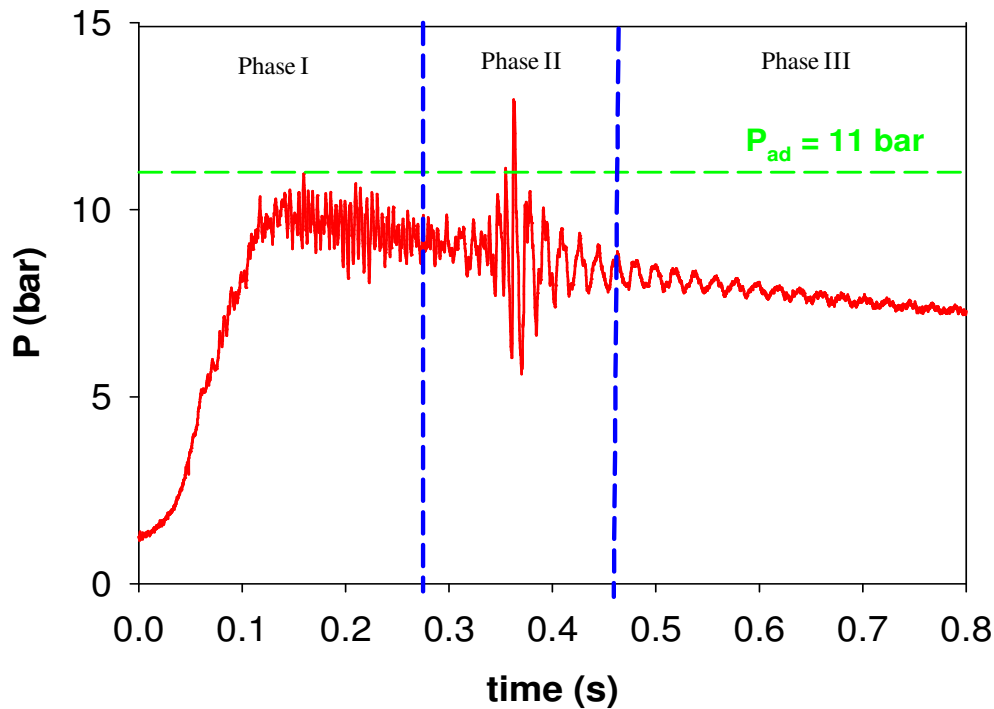


Figure 8. Pressure time history for stoichiometric $\text{CH}_4/\text{O}_2/\text{N}_2$ with $E=0.40$ as measured by Di Benedetto et al. (2011).

The authors addressed the nature of the anomalous behavior to a coupling of a deflagration and a rapid phase transition (RPT) of the water produced by combustion reaction, in particular to cycles of condensation and vaporization of the water produced during the flame propagation. More specifically, when a liquid is heated to its boiling point, in the absence of nucleation sites, it may undergo superheating without boiling [Reid, 1976; 1983]. Super-heating may proceed up to a limit temperature (super-heating temperature) above which RPT occurs. The vapor expansion associated with RPT generates rapid increase in pressure, eventually leading to the formation of shock waves.

According to Di Benedetto et al. (2011) the combustion water condenses at the vessel walls and due to the radiation heat coming from the flame, starts to evaporate explosively, if superheated. This rapid phase transition of water produces shock waves which drive to over-adiabatic pressure peaks, hence the phenomenon has been named combustion-induced Rapid Phase Transition (c-RPT).

The occurrence and the severity of the c-RPT phenomenon has been found to be dependent on the quantity and nature of diluents (Ar, He, N₂ and CO₂ were tested) and on the vessel surface to volume ratio [Di Benedetto et al. 2012a]. Indeed, it was showed that c-RPT severity increases with the surface to volume ratio of the vessel. Furthermore, it has been found the disappearing of the c-RPT phenomenon by sprinkling ultra-fine Mg₃Si₄O₁₀(OH)₂ powder over the vessel walls which prevents explosive water evaporation providing nucleation sites, as showed in Figure 9 (Salzano et al., 2013). The red and blue curves represent the pressure time histories of CH₄/O₂/N₂/CO₂ mixture (molar ratios equal to 1/2/1.33/1.08) exploding in a 5L closed vessel in absence and presence of talc on internal surface of the reactor, respectively. The presence of talc enables water evaporation. No super-heating and no RPT. The peak pressure decreases reaching a value close to the adiabatic one.

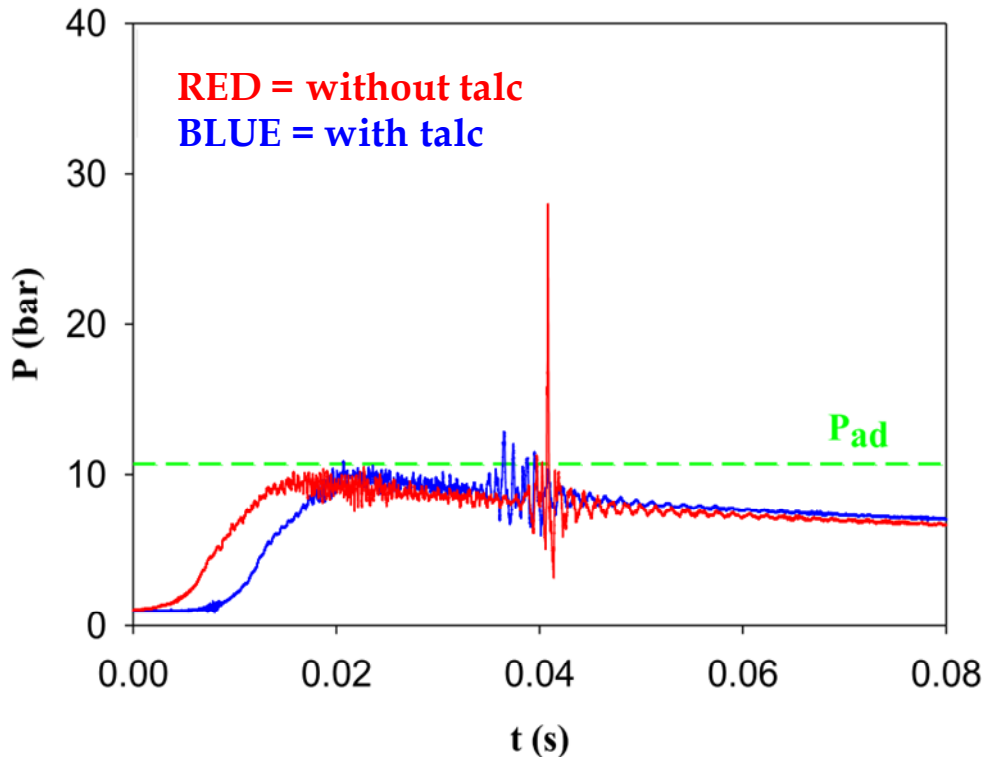


Figure 9. Pressure histories of $CH_4/O_2/N_2/CO_2$ mixture (molar ratios equal to 1/2/1.33/1.08) in a closed vessel in absence and presence of talc [Salzano et al. 2013]

Finally, when heating the reactor walls at temperatures higher than the water condensation temperature, c-RPT does not occur as showed in Figure 10 (Di Benedetto et al., 2011) in the case of explosion of a CH_4/O_2 mixture (CH_4/O_2 molar ratio = $1/2$) in a closed vessel. In particular, when the wall temperature (T_{wall}) is maintained at 273K or 423K, partial pressure of the water (P_{H_2O}) produced as calculated at adiabatic conditions, is greater than Water vapor pressure ($P^{\circ}_{H_2O}$) at T_{wall} and c-RPT is manifested. As wall is heated until a temperature of 473K, P_{H_2O} results minor than $P^{\circ}_{H_2O}$ at T_{wall} and c-RPT behavior disappears.

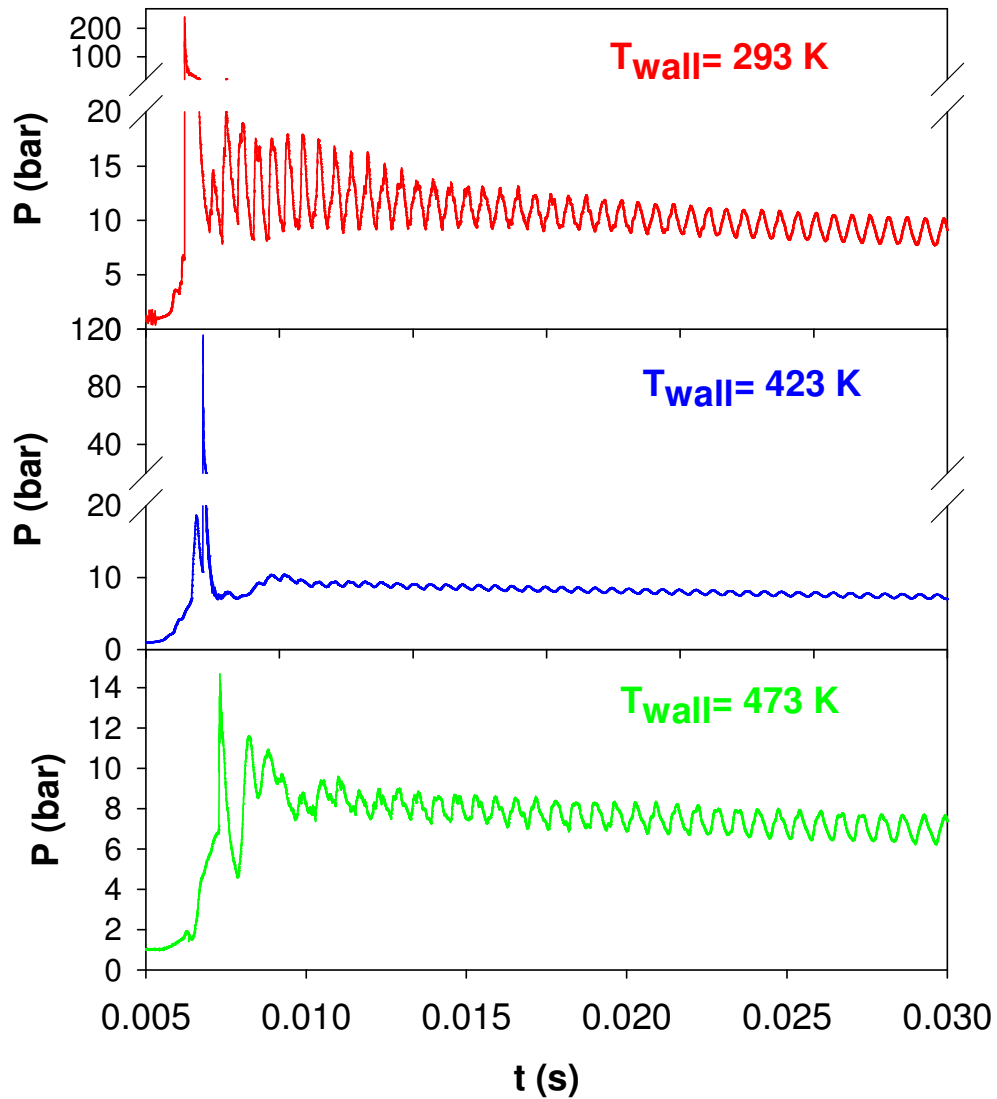


Figure 10. Pressure histories of CH_4/O_2 mixtures (33.3%/66.7% molar composition) by varying wall temperature of the reactor vessel

From the literature results it appears that when burning in oxygen enriched air rather than pure air, the quantitative and qualitative behavior during explosion changes completely. Open questions about the nature and occurrence of this anomalous behavior, which has been named “heat explosion” or “c-RPT” still exist and have been analyzed in this work .

3. AIM OF THE WORK

The aim of this PhD thesis is to evaluate the occurrence and severity of c-RPT phenomenon for $H_2/CO/O_2/N_2/CO_2$ mixtures. To this aim, research activity has been divided in two parts.

The first part of activity has been focused on the characterization of the reactivity and explosive behavior of the mixtures of interest evaluating the combined effects of composition (inerts, CO_2 and O_2 content) temperature and pressure. Explosion parameters (maximum pressure, maximum rate of pressure rise, burning velocity) for $H_2/CO/O_2/N_2/CO_2$ mixtures were evaluated by varying the following parameters:

- i) fuel composition
- ii) fuel (H_2+CO) concentration with respect to O_2 expressed as equivalence factor ϕ :

$$\phi = \frac{\left(\frac{H_2 + CO}{O_2} \right)}{\left(\frac{H_2 + CO}{O_2} \right)_{st}} \quad (2)$$

- iii) CO_2 content (or inert species) in the mixture
- iv) level of oxygen-enrichment expressed in terms of enrichment factor E (in the range between 0.21, i.e. air, and 1, i.e pure oxygen):

$$E = \frac{O_2}{O_2 + N_2} \quad (3)$$

To this regard, a methodical experimental and numerical study was performed focalizing on flame propagation phenomenon at atmospheric conditions of temperature and pressure and to c-RPT occurrence.

The second part of the activity has been focused on the quantification of the key role of water produced by combustion reaction in driving the c-RPT phenomenon. To this aim stoichiometric CO/O₂/N₂ mixtures, by varying the oxygen enrichment factor E from 0.21 (air) to 1 (pure oxygen), in the presence and in the absence of H₂ have been experimentally tested.

A theoretical analysis, based on the definition of dimensionless characteristic time ratios, has been conducted in order to predict on the occurrence and severity of c-RPT phenomenon.

In the light of this theoretical study, experimental results obtained in the open literature have been analyzed.

4. METHODS

The research activity here proposed is prevalently based on experiments and numerical computations and make use of equipment and devices available in the laboratory of the Istituto di Ricerche sulla Combustione, Consiglio Nazionale delle Ricerche (CNR-IRC) in Naples (IT).

4.1. Experimental

The experimental apparatus adopted is shown in Figure 11, where is reported a photograph of the cylindrical vessel.



Figure 11. High pressure cylindrical vessel

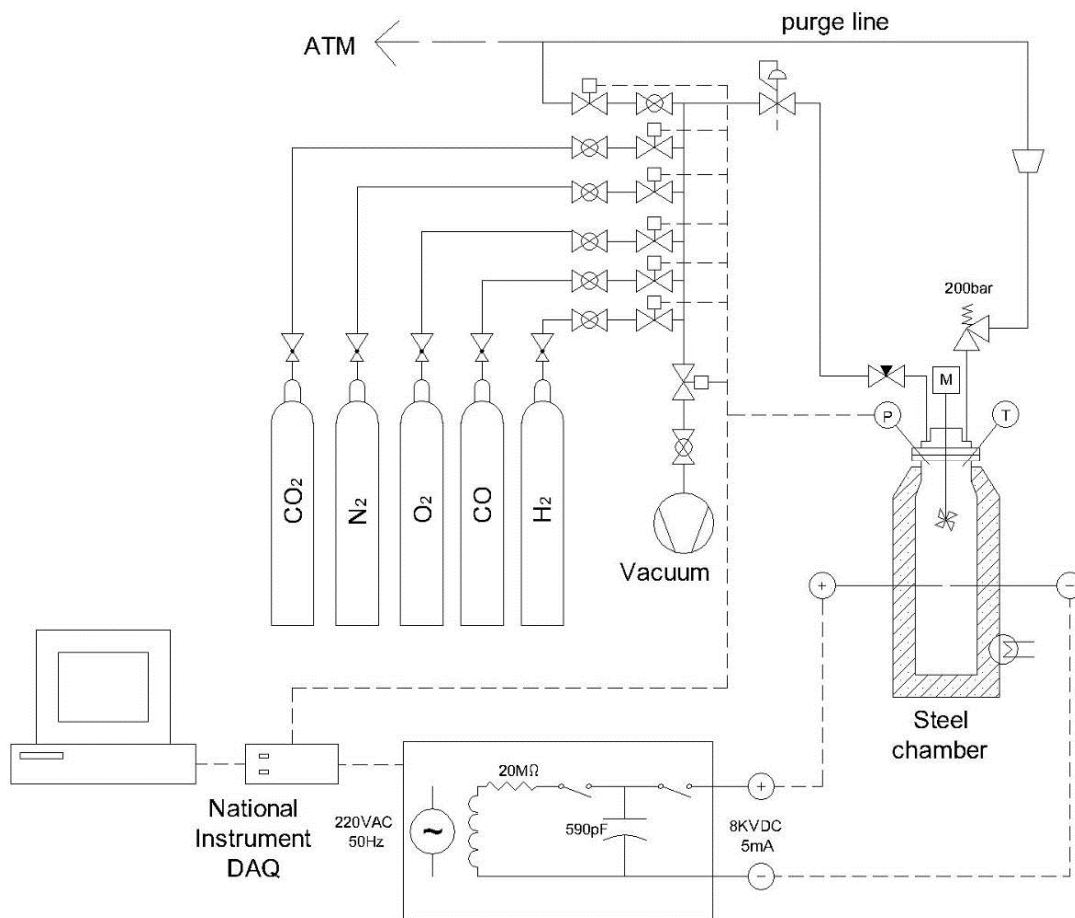


Figure 12. The experimental scheme adopted for this study: cylindrical vessel.

The main reactor is composed by a AISI 316 SS steel, cylindrical vessel (5 L), wall thickness of 5 cm. Maximum allowable working pressure was tested at 400 bar. The mixture composition was obtained by the partial pressure method. Gases were premixed by mechanical stirring (rotating shaft velocity equal to 200 rpm). They were allowed to settle for around 30 s and then ignited by an electric spark (25 kV, 30 mA) positioned at the center of the vessel. Pressure histories were recorded by KULITE ETS-IA-375 (M) series transducers fed by chemical battery (12 VDC/7 Ah) in order to minimize any disturbance on the output supply, which was recorded by means of a National Instrument USB-6251 data acquisition system (1.25 Msamples/sec).



Figure 13. High pressure tubular vessel

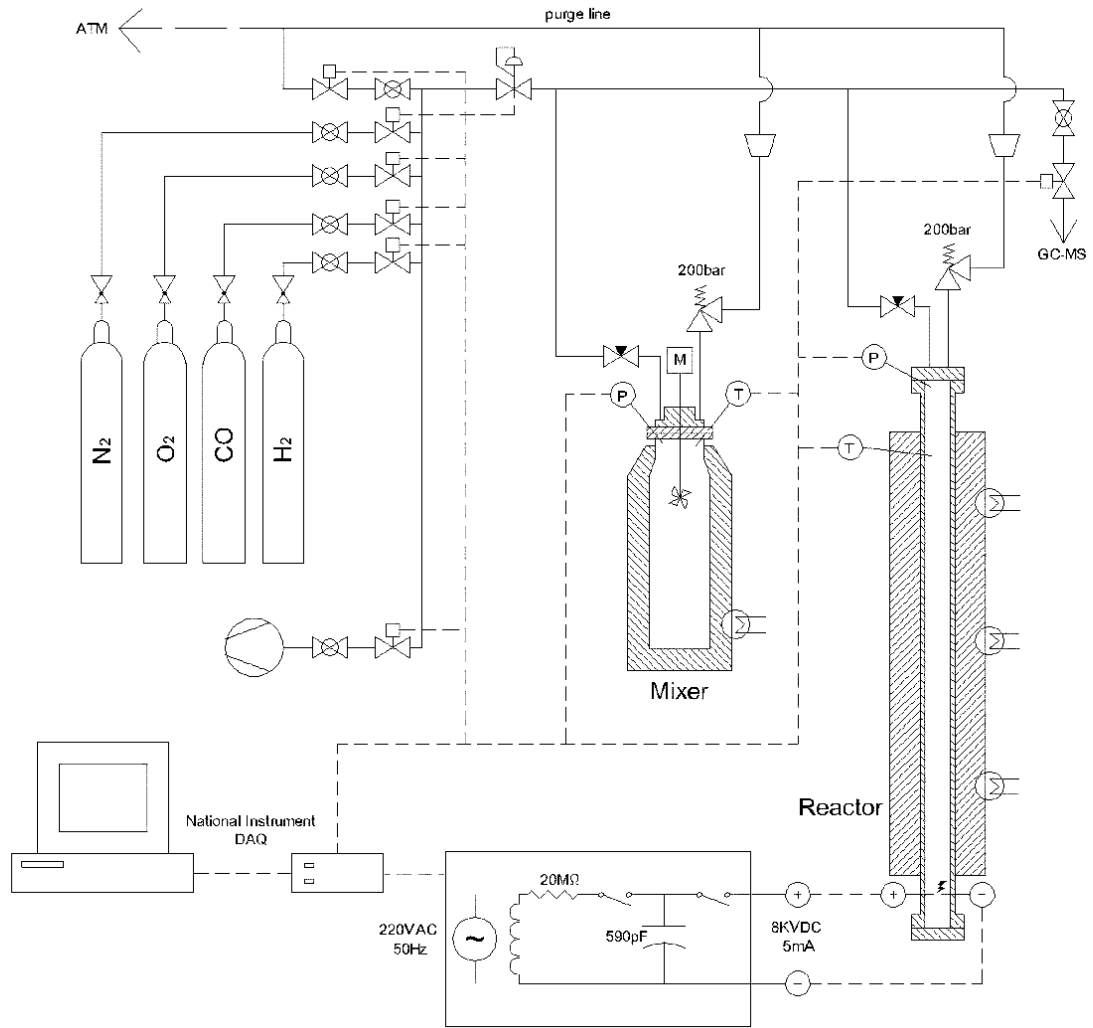


Figure 14. The experimental scheme adopted for this study: tubular vessel.

The system showed in Figure 14 is composed by two sections: a mixer for the preparation of the reactive mixture and a reactor for the explosion test (Figure 13).

The mixer consists of a 5 dm³, cylindrical vessel and includes a magnetic-driven stirring system for mixing. The reactor reported in Figure 13, consists of a cylindrical AISI316SS stainless-steel, wall thickness 5 cm. The diameter is 6 cm, and the vertical length is 120 cm. The reactor is equipped with rupture disk, the maximum allowable operating pressure is 200 bar. For pressure recording, which is the core measurement for the experiments reported in this work, a Kulite ETS-IA-375 (M) series pressure transducer with a natural frequency of 150 kHz has been used. These transducers are specifically designed for high-

pressure, high- shock environments and blast analysis. The electrical power for the transducer has been supplied by means of a chemical battery 12 VDC/7 AH in order to minimize any disturbance on the output current, which has been recorded by means of a National Instrument USB- 6251 data acquisition system (16 bit, 1.25×10^6 samples/s), with a frequency up to 1.0 MHz. No manipulations were performed on the analogical signal output from the transducer or the digital data recorded. Hence, data show large oscillations due to observation (or additive) and dynamic noise. The data have been than filtered by using non-linear algorithm based on Savitzky–Golay (SG) method [Savitzky & Golay, 1964], which utilizes an array of weighted coefficients as a smoothing function to convolute m uniformly spaced neighbouring points. In the following, we have used $m = 21$, a typical value adopted in explosion science.

The fuel–oxidant mixtures used in this work were obtained by the partial pressure methodology. The mixture obtained was sent to the tubular reactor and the gases were ignited by a single spark [8 kV direct current (DC)] through two electrodes positioned at the bottom of the equipment (spark gap = 1 mm). To this aim, a RC circuit (Capacitor = 590 pF; Current Intensity: 5 mA), by using PC-based automatic reed relays as high-voltage switch. The estimated energy is 20 mJ.

From the pressure histories obtained by the experimental tests, laminar burning velocities have been calculated. In a great number of literature studies, the laminar burning velocity of a combustible mixture was obtained from the time evolution of the radius of spherically expanding flame, captured by means of high-speed photographic techniques [Kim et al. 2002, Chen et al. 2007, Law et al. 2004, Tang et al. 2009]. However, the laminar burning velocity can be obtained from the time pressure record of explosion occurring in closed vessel [Lewis & Von Elbe, 1961]. In particular, the equations of Dahoe et al. (2003, 2005)

which link the flame radius, r_f and the laminar burning velocity, S_l , to the pressure time history will be used. The flame radius will be calculated by using the following correlation:

$$r_f = \left(\frac{3V}{4\pi} \right)^{1/3} \left[1 - \left(\frac{P^\circ}{P} \right)^{1/\gamma} \left(\frac{P_{\max} - P}{P_{\max} - P^\circ} \right) \right]^{1/3} \quad (4)$$

where γ is the heat capacity ratio, P_{\max} is the maximum measured pressure, P° is the initial pressure, and V is the vessel volume. The (un-stretched) laminar burning velocity S_l will be then calculated according to:

$$S_l = \lim_{r_f \rightarrow r_f^\circ} \left[\frac{d}{dt} r(t) \right]_{\Delta r_f} \quad (5)$$

where $r(t)$ is the best fit function in the range $\Delta r_f = (r_f - r_f^\circ)$, which refers to the range of the flame radius for which either ignition or the wall effects and vessel shape can be neglected on the flame propagation. The boundaries of this range have been evaluated by considering the places where the time derivative of radius is always positive with radius, i.e.:

$$\frac{d}{dr} \left(\frac{dr}{dt} \right)_{\Delta r_f} \geq 0 \quad (6)$$

The value of S_l corresponds to the un-stretched burning velocity as in Huang et al. (2006). As also shown by Dahoe (2005), the values of S_l calculated by means of this methodology do not significantly differ from the values reported in the literature and measured with more advanced techniques, such as photographs of the propagating flame.

4.2. Model

The numerical calculation of the laminar burning velocities of the mixtures were carried out by means of simulation of the one-dimensional, planar, adiabatic, steady, un-stretched, laminar flame propagation. To this aim, the Sandia PREMIX module [Kee et al., 1985] of the CHEMKIN package will be, coupled to the detailed Davis reaction scheme [Davis et al., 2005].

The code, which adopts a hybrid time-integration/Newton-iteration technique to solve the steady-state mass, species, and energy conservation equations, was set up to simulate a freely propagating flame with mixture-averaged formulas. The initial flow rate of the unburned mixture was set to $0.04 \text{ g/cm}^2 \text{ s}$ [Di Sarli & Di Benedetto, 2007]. At the inlet boundary, pressure, temperature and composition of the fresh mixture were assigned. At the exit boundary, all gradients were imposed to vanish.

The adopted type of formulation requires an additional boundary condition for the mass flow rate that was assigned by fixing the flame location and, in particular, the point at which the flame temperature reaches the value equal to 400 K. To start the iteration, the temperature profile estimation obtained by Van Maaren et al. (1994) for stoichiometric methane/air flame was adopted, as suggested by Uykur et al. (2001). The temperature profile resulting from the first simulation step was used for the next step.

In the computations, the windward differencing on both convective and diffusion terms was used. The model uses a non-uniform grid that is successively and automatically adapted based on solution gradients determined on an initially coarse grid. Relative gradient and curvature parameters, which determine the extent to which the solution is refined for each case, have to be provided. The total length of the calculation domain, starting 2 cm upstream of the reaction zone, was chosen equal to 12 cm. Further increases

in mesh resolution and domain-size resulted in less than 1 cm/s difference in the calculated flame speeds.

4.3. Thermochemical analysis

The two essential parameters for the study of combustion systems are namely the equilibrium product temperature and composition. If all the heat evolved in the reaction is employed to raise the product temperature, this temperature is called the adiabatic flame temperature, T_{ad} . Because of the importance of the temperature and gas composition in combustion considerations, it is appropriate to review those aspects of the field of chemical thermodynamics that deal with these subjects.

All chemical reactions are accompanied by either an absorption or evolution of energy, which usually manifests itself as heat. It is possible to determine this amount of heat and hence the temperature and product composition from very basic principles.

The internal energy U of a given substance is found to be dependent upon its temperature, pressure, and state and is independent of the means by which the state is attained. The change of the internal energy dU of a system is given by the sum of the heat dQ transferred and the work dW done to the system,

$$dU = dQ + dW \tag{7}$$

Work can be added to a system in various ways, in this study it is assumed compression work only.

$$dU = dQ - pdV \tag{8}$$

for constant volume V the change of internal energy equals the heat transferred

$$dU = dQ \quad (9)$$

when heat is transferred to a system, the temperature changes. The heat capacity C_v of a system at constant volume is defined as:

$$C_v = \frac{dU}{dT} \quad (10)$$

the first law of thermodynamics becomes:

$$dU = dQ = C_v dT \quad (11)$$

with the knowledge of C_v , the internal energy U can be determined at every temperature:

$$U_T = U_{Tref} + \int_{Tref}^T C_v dT \quad (12)$$

The internal energy change in a chemical reaction

$$v_1 A_1 + v_2 A_2 + v_3 A_3 + \dots + v_i A_i = 0 \quad (13)$$

where A_i denotes the chemical compound and v_i the stoichiometric coefficient, is given by the sum of internal energies times the corresponding stoichiometric coefficients

$$\Delta U = \sum_{i=1}^S v_i U_i \quad (14)$$

The determination of the adiabatic temperature T_{ad} at constant V is obtained by imposing

$$\Delta U = 0 \quad (15)$$

The calculation of equilibrium composition at constant V of the burnt gases in combustion process of $\text{CO}/\text{H}_2/\text{O}_2/\text{N}_2$ mixture has been performed on the basis of the principle of the minimization of free energy of Helmholtz A , according the following steps [Warnatz et al. 2006]:

Choice of the chemical system

First, the number S of different compounds in the reaction system must be determined. All species relevant to the system have to be considered. In the specific case of this study, in order to describe the relevant species in the burnt gas of a stoichiometric mixtures one needs the compounds:



That means that we need 5 equations to determine the equilibrium composition.

Determination of the components of the system

Each mixture of S species (compounds) has a certain number K of components (chemical elements). These components are conserved.

In our system there are $K = 3$ different elements (C, H, O).

The molar balances on these four elements give 4 equation to solve the problem

Determination of the independent reactions

The compounds in the system which have not been chosen as components can change due to chemical reactions. Therefore $R = S - K$ independent chemical equilibrium conditions have to be specified. In this study $R = 5 - 3 = 2$ independent reaction:



For each reaction it can be written an equilibrium equation:

$$K_{Ci} = \prod_i \left(\frac{c_i}{c_o} \right)^{v_i} \quad (19)$$

Solution of the equation system

There are 3 equations on the elements and 2 equilibrium equations for 5 chemical compound to determine: the system is determined.

5. RESULTS

In this section, the study on the characterization of the reactivity and explosive behavior of $H_2/CO/O_2/N_2/CO_2$ mixture and the analysis of the explosion behavior of stoichiometric $CO/H_2/O_2/N_2$ mixtures, by varying either the oxygen enrichment factor from 0.21 (air) to 1 (pure oxygen), and the hydrogen to carbon monoxide ratio are reported.

5.1. Explosive behavior of $H_2/CO/O_2/N_2/CO_2$ mixture

Table 4 reports the mixture compositions investigated in the first part of this thesis, together with the corresponding values of adiabatic temperature (T_{ad}) and pressure (P_{ad}) at constant volume, as computed by the Gaseq Chemical Equilibrium Program [GASEQ, 2011].

Table 4. The syngas compositions analyzed and tested experimentally. Y is the molar fraction. T_{ad} , P_{ad} are respectively the adiabatic flame temperature and pressure as calculated by GASEQ. Test 1: no CO_2 .

Test	ϕ	H_2/CO	$E=O_2/(O_2+N_2)$	Y_{H_2}	Y_{CO}	Y_{O_2}	P_{ad} , bar	T_{ad} , K
1	1.00	1	0.21	0.148	0.148	0.148	7.9	2700
2	1.00	1	0.21	0.089	0.089	0.089	5.2	1719
3	1.00	1	0.60	0.164	0.164	0.164	6.9	2426
4	1.00	2	0.21	0.118	0.059	0.089	5.2	1695
5	1.00	2	0.60	0.218	0.109	0.164	6.9	2416
6	1.75	1	0.21	0.127	0.127	0.073	4.5	1469
7	1.75	1	0.60	0.203	0.203	0.116	6.0	2044
8	1.75	2	0.21	0.169	0.085	0.073	4.5	1440
9	1.75	2	0.60	0.271	0.135	0.116	5.9	2009

The value of equivalence ratio corresponding to fuel-rich mixtures ($\phi = 1.75$) has been considered because it corresponds to the maximum value for the laminar burning velocity measured by several other authors by using air as oxidant (see e.g. Natarajan et al., (2007)). In the following, the experimental results are first presented. Hence, the model results for the laminar burning velocity are compared to experimental data.

5.1.1. Effect of E, ϕ and H₂/CO ratio

Figure 15 the experimental pressure time histories are shown at changing the oxygen-air enrichment (E), at different values of the equivalence ratio (ϕ) and H₂/CO ratio, (40 % of CO₂). The effect of the oxygen-enrichment is seen in the top part of the figure, where the increased reactivity and larger enthalpy of combustion of the fuel mixture is evident in the shorter duration of the overall explosion phenomenon and the higher maximum pressure obtained in the case of E = 0.6 with respect to air. Similar results are also evident in the case of rich fuel concentration or for higher H₂ content, as seen in the middle and bottom part of the same Figure.

In Figure 16, the effect of the equivalence ratio on the explosion behavior of syngas mixtures is shown in air (E = 0.21) and oxygen-air enrichment (E = 0.6), in the presence of 40 % CO₂. For E = 0.21 (Figure 16 top), both the maximum pressure and the rate of pressure rise are higher at stoichiometric conditions ($\phi = 1$) than at rich conditions ($\phi = 1.75$). At higher oxygen-enrichment (E = 0.6), the effect of equivalence ratio is marginal either on the pressure history or on the reactivity of the fuel.

Finally, Figure 17 shows the effect of the H₂/CO ratio on the pressure history either for stoichiometric syngas-air mixtures (Tests 2-4) or for rich composition (Tests 6-8). For the syngas-air mixtures (E = 0.21) the effects of the hydrogen content on the pressure histories is negligible.

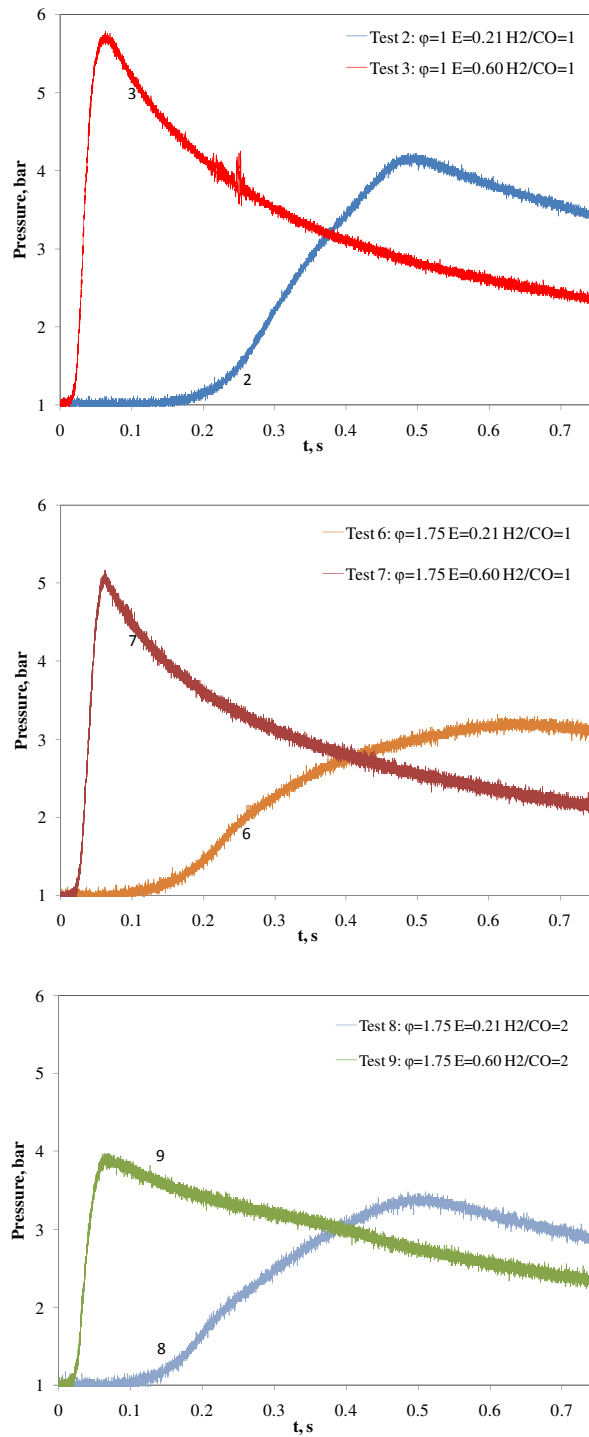


Figure 15. Effect of oxygen-enrichment. $CO_2=40\%$ v/v. Top: Effect of oxygen-enrichment factor for the stoichiometric concentration of fuel (H_2+CO). Composition blue line: 8.9% H_2 , 8.9% CO , 8.9% O_2 ; Composition red line: 16.4% H_2 , 16.4% CO , 16.4% O_2 . Middle: As top figure, for rich concentration of fuel (H_2+CO) in air. Composition orange line: 12.7% H_2 , 12.7% CO , 7.3% O_2 ; Composition red line: 20.3% H_2 , 20.3% CO , 11.6% O_2 . Bottom. Effect of (H_2/CO) ratio. Composition blue line: 16.9% H_2 , 8.5% CO , 7.3% O_2 ; Composition green line: 27.1% H_2 , 13.5% CO , 11.6% O_2 .

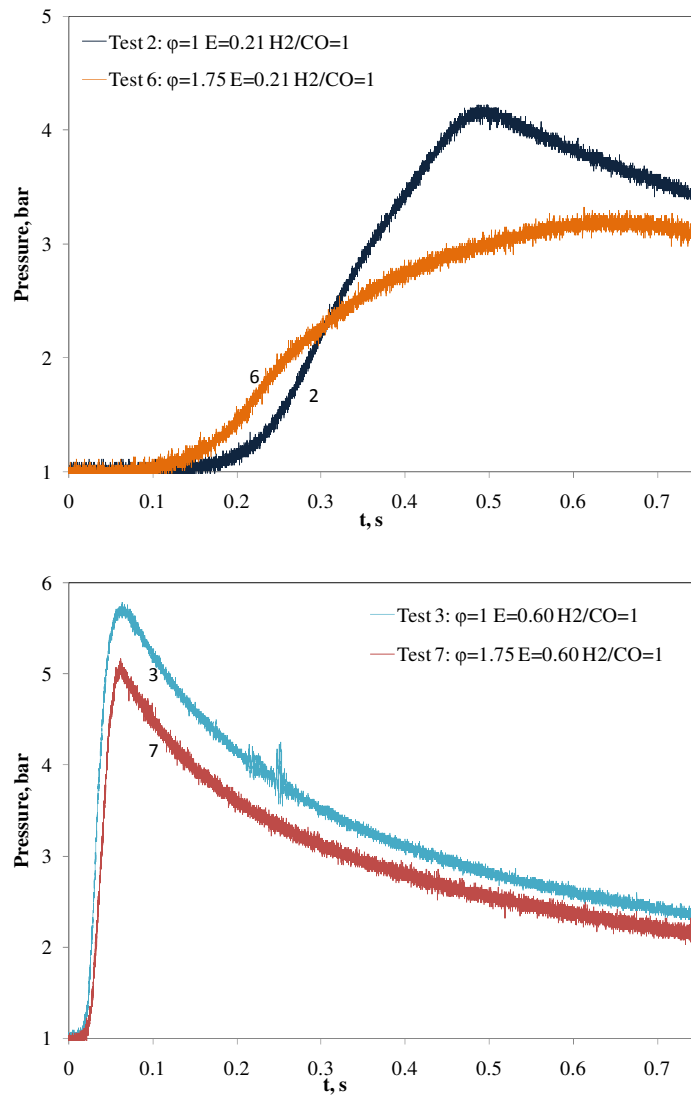


Figure 16. Effect of equivalence ratio for different oxygen-enrichment E . $CO_2=40\%$ v/v.
 Top: Effect of equivalence ratio in air. Composition black line: 8.9% H_2 , 8.9% CO , 8.9% O_2 ; Composition orange line: 12.7% H_2 , 12.7% CO , 7.3% O_2
 Bottom: Effect of equivalence ratio in oxygen-enriched air ($E = 0.6$). Composition blue line: 16.4% H_2 , 16.4% CO , 16.4% O_2 ; Composition red line: 20.3% H_2 , 20.3% CO , 11.6% O_2 .

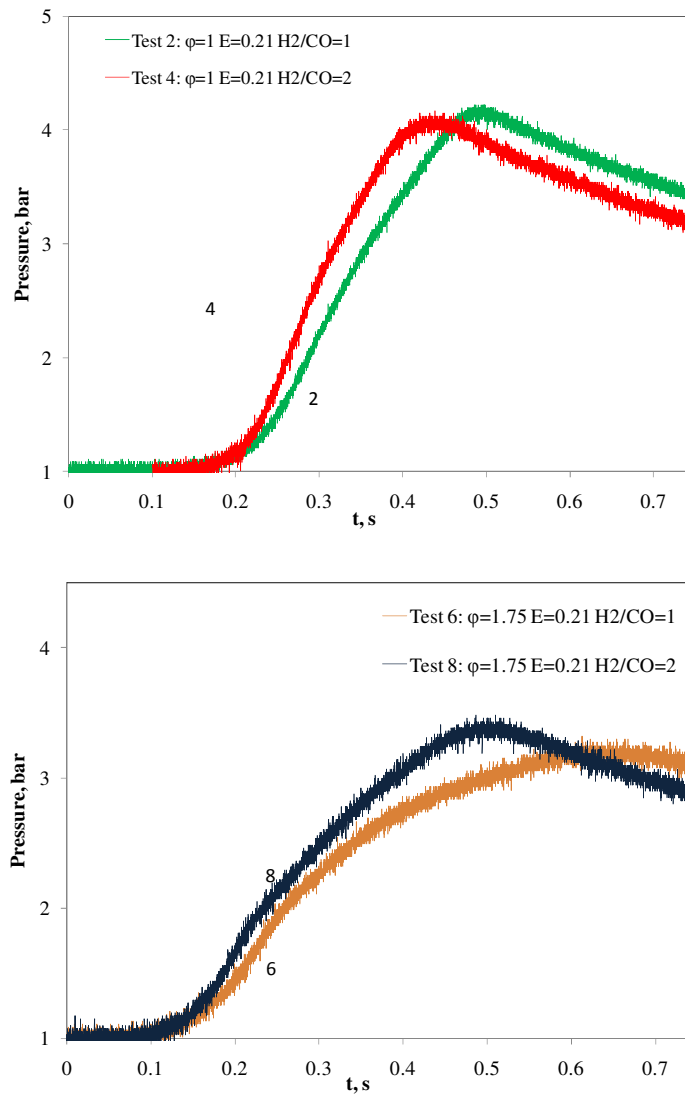


Figure 17. Effects of hydrogen enrichment. $CO_2=40\%$ v/v. Top: Effect of H_2/CO ratio for stoichiometric fuel in air. Composition green line: 8.9% H_2 , 8.9% CO , 8.9% O_2 ; Composition red line: 11.8% H_2 , 5.9% CO , 8.9% O_2
 Bottom: Effect of H_2/CO ratio for rich concentration of fuel in air. Composition orange line: 12.7% H_2 , 12.7% CO , 7.3% O_2 ; Composition black line: 16.9% H_2 , 8.5% CO , 7.3% O_2 .

5.1.2. Laminar burning velocity

For the compositions given in Table 4, the maximum pressure (P_{max}) and the laminar burning velocities (S_l) calculated through Eqs. 4, 5 from the experimental pressure time histories obtained in the high pressure cylindrical reactor (Figures 15-17) are given in Table 5.

Table 5. Maximum pressure and laminar burning velocity for the mixtures of Table 1. Test 1: no CO_2 .

Test	ϕ	H_2/CO	$E=O_2/(O_2+N_2)$	P_{max} bar	S_l , $cm\ s^{-1}$
1	1	1	0.21	6.31 ± 0.03	97.5 ± 8.2
2	1	1	0.21	4.15 ± 0.02	6.5 ± 1.9
3	1	1	0.60	5.67 ± 0.03	67.6 ± 2.8
4	1	2	0.21	4.08 ± 0.02	8.3 ± 2.7
5	1	2	0.60	6.16 ± 0.03	80.2 ± 7.1
6	1.75	1	0.21	3.29 ± 0.14	13.2 ± 1.7
7	1.75	1	0.60	5.16 ± 0.13	77.5 ± 8.4
8	1.75	2	0.21	3.42 ± 0.06	10.3 ± 0.6
9	1.75	2	0.60	4.00 ± 0.14	90.13 ± 6.00

The data in the table show that the laminar burning velocity for the oxygen enriched tests ($E = 0.6$) is one order of magnitude larger than the burning velocity obtained in pure air, whatever the equivalence ratio (ϕ) and the H_2/CO ratio. In the presence of CO_2 , the calculated laminar burning velocity is higher at $\phi = 1.75$ than at $\phi = 1$. These results are in agreement with the findings of Lieuwen et al. (2010) and Mclean et al. (1994) on syngas explosion in air.

These results can be compared with the values calculated by Chemkin analysis. The computed values of the laminar burning velocity by varying the equivalence ratio for

different values of the oxygen-enrichment factor (E) and H_2/CO ratios are shown in Figure 18. Experimental values (Table 5) are also shown.

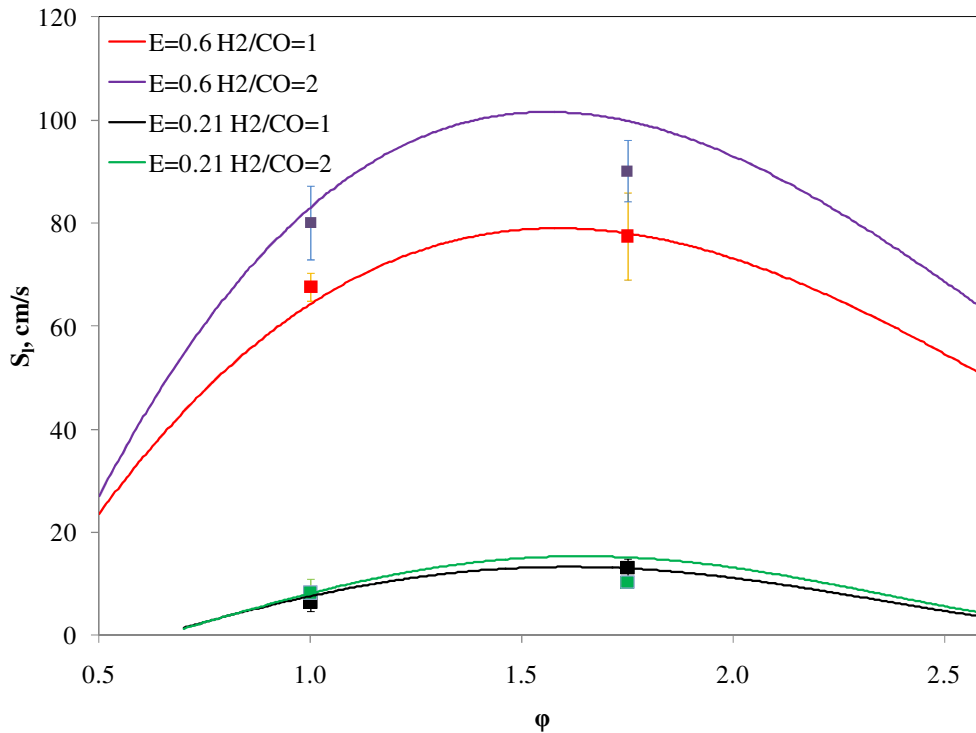


Figure 18. Laminar burning velocity S_b for the syngas explosion vs. equivalence ratio ϕ , by varying H_2/CO ratio, oxygen-enrichment factor E , $CO_2 = 40\%$ v/v. Experimental tests as in Table 2 are reported for the sake of validation.

The calculated values of burning velocity agree quite well with experimental data. The maximum values of the laminar burning velocity are found at rich conditions and in particular at about ($\phi = 1.6$). Such values slightly depends on the oxygen-air enrichment (E) and on the H_2/CO ratio.

On increasing the oxygen content (i.e., on increasing E), the values of the laminar burning velocity increases from about 5-10 cm/s up to 80-100 cm/s.

It is worth noting that the main finality of the model simulation has been the validation of Davis mechanism respect my experimental study so that I could calculate values of laminar burning velocity for theoretical evaluations reported in the second part of this thesis.

5.1.3. Effect of CO₂

Figure 19 shows the calculated values of the laminar burning velocity as function of the CO₂ content. In the same figure, the experimental data of Table 5 and literature data are also shown. The comparison between the computed values and the experimental data are in a good agreement, suggesting that the Davis mechanism is adequate for simulating the laminar burning velocity also in oxygen-air enrichment conditions.

The CO₂ addition significantly reduces the laminar burning velocity up to extinguishing it (CO₂ ~ 60 %; S₁ ~ 50 mm/s).

This result was previously found also for CH₄/O₂/N₂/CO₂ and H₂/O₂/N₂/CO₂ mixtures [Di Benedetto et al., 2009]. For these mixtures, Di Benedetto et al. (2009) also put in evidence that the main role played by CO₂ is thermal rather than kinetic, as it decreases the flame temperature.

In this work we investigated the nature of the role of CO₂. To this end, we performed *ad hoc* simulations by artificially suppressing the kinetics of CO₂ without varying the thermodynamic properties of the same substance.

In Figure 19 the laminar burning velocity values obtained by suppressing the kinetic role of CO₂ are shown (---). It appears that the kinetic effects is relevant for higher CO₂ concentrations. CO₂ behaves as a competitor in the mechanism by reducing the overall reactivity.

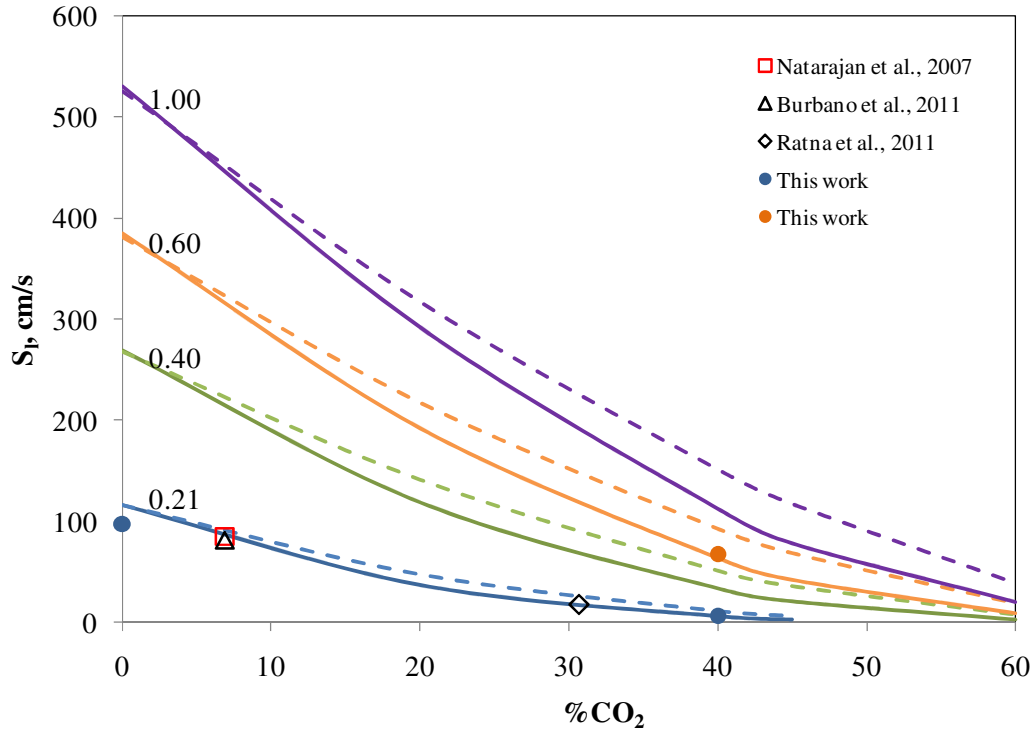


Figure 19. Laminar burning velocity for syngas composition vs. CO_2 concentration for different oxygen-enrichment factor E . $\text{H}_2/\text{CO} = 1$, $\phi = 1$. Dashed lines represent the calculated values obtained by using a reactivity-inert species in place of CO_2 .

Similar behavior was found for $\text{H}_2/\text{CO} = 2$ and $\phi = 1.75$; results are not reported here for the sake of brevity.

In order to quantify the weight the kinetic and thermal role of CO_2 on the laminar burning velocity, we computed the relative increment ($\Delta S_L/S_L$) of the burning velocity between real values (i.e. including kinetic and thermal effects) and the artificial values (i.e. neglecting the kinetic effect).

In Figure 20 $\Delta S_L/S_L$ is plotted versus the actual value of S_L .

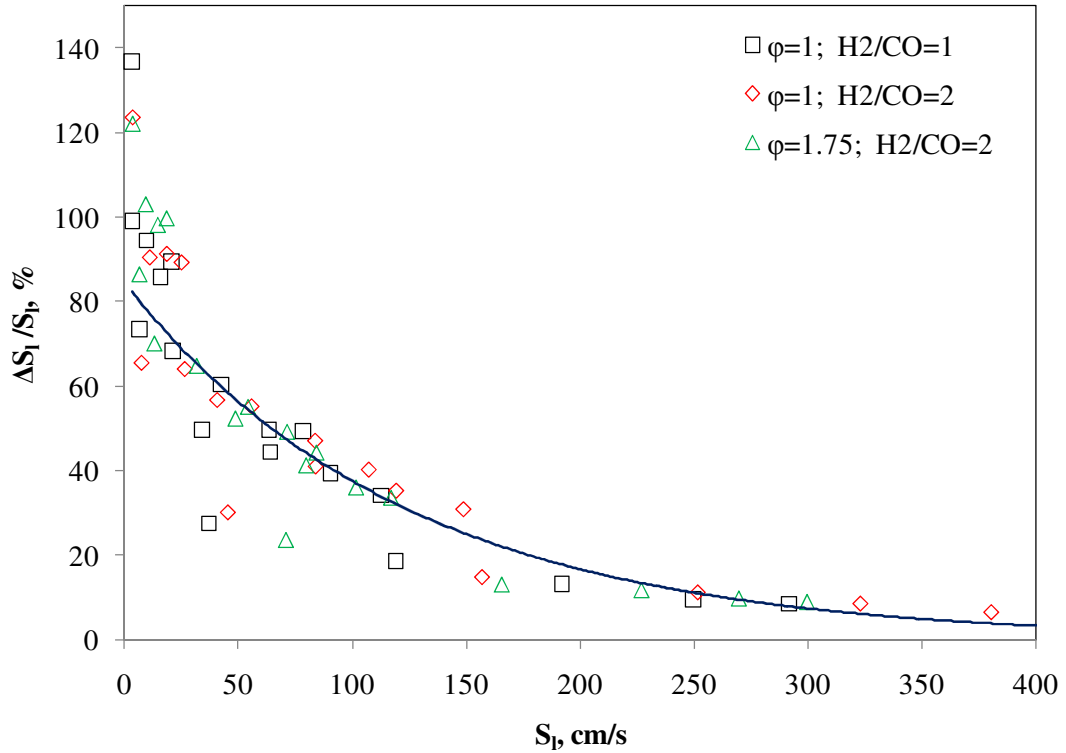


Figure 20. Relative increment of calculated burning velocity for syngas combustion with CO_2 with respect to the equivalent mixture with inert- CO_2 . CO_2 content ranges from 0% to 60% v/v.

From Figure 20, it appears that the kinetic effect of CO_2 is higher at low reactivity i.e.

$S_1 \rightarrow 0$ cm/s (i.e. low O_2 enrichment, or high CO_2 content or equivalent ratio ϕ).

The role of CO_2 is mainly thermal for highly reactive mixtures (S_1 values higher than 200 cm/s), where hydrogen effects are dominant.

5.1.4. Correlation for laminar burning velocity

Figures 21 and 22 shows the burning velocity as calculated by using the CHEMKIN code for the syngas mixture, with or without CO₂ (40% v/v), by varying H₂/CO ratio and the oxygen-air enrichment (E).

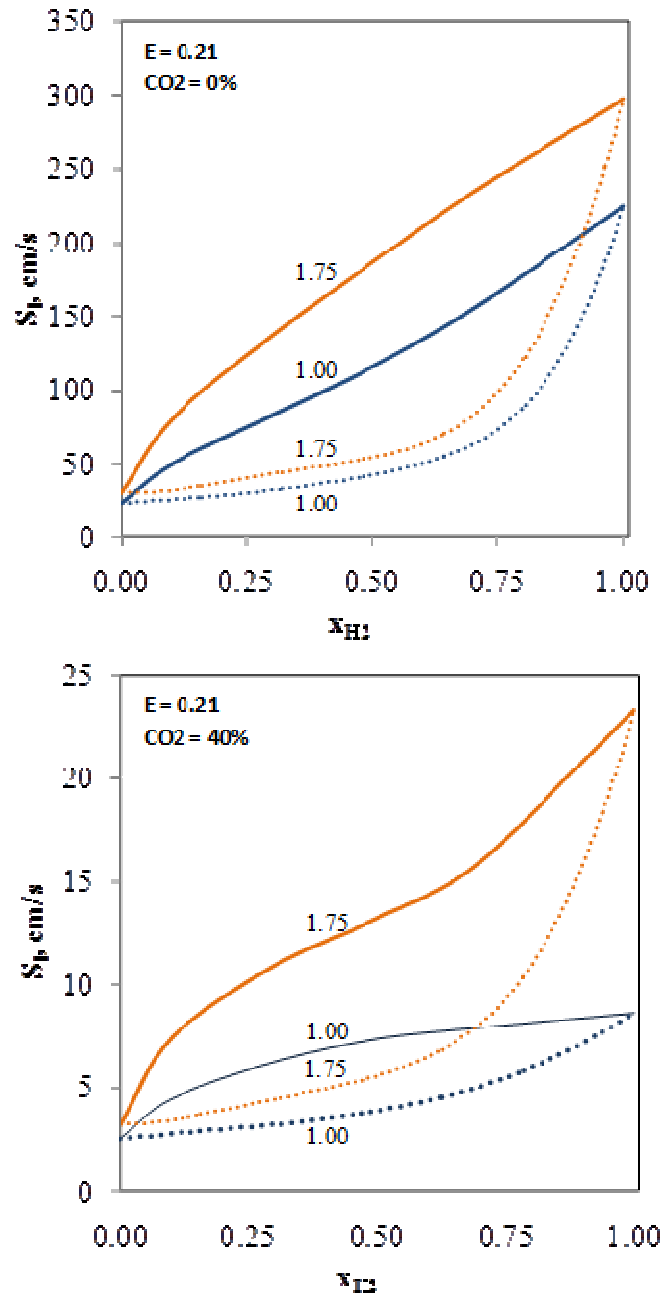


Figure 21. Calculated burning velocity for syngas combustion either without CO₂ or with CO₂ 40% v/v by varying H₂/CO ratio, for two fuel (H₂+CO) equivalence ratios (namely 1 and 1.75) ; E=0.21. Le Chatelier curves are also included (dotted line).

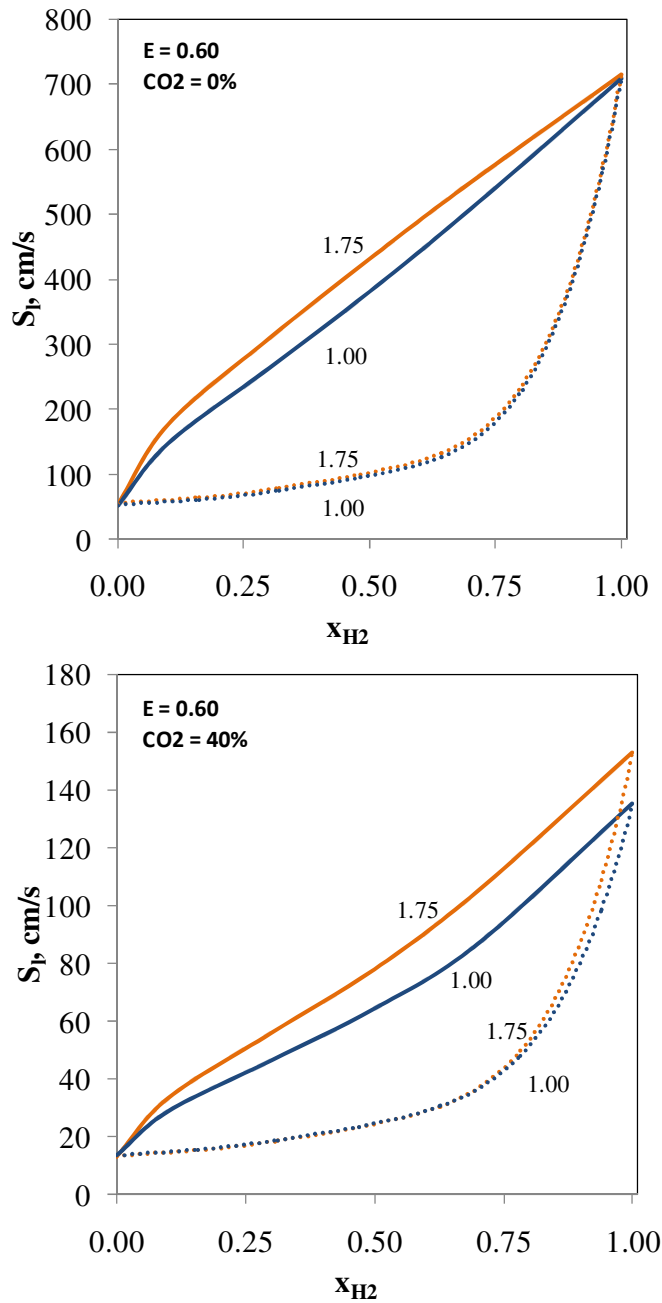


Figure 22. Calculated burning velocity for syngas combustion either without CO_2 or with CO_2 40% v/v by varying H_2/CO ratio, for two fuel (H_2+CO) equivalence ratios (namely 1 and 1.75) ; $E=0.60$. Le Chatelier curves are also included (dotted line).

In the absence of CO_2 , (Figures 21-22, top), the laminar burning velocity is a linear combination of H_2 and CO content, whatever the equivalence ratio and the oxygen content.

The value of the laminar burning velocity of the syngas mixtures, may be then computed via the following equation:

$$S_l(\varphi, air) = S_{l,CO}(\varphi)x_{CO} + S_{l,H_2}(\varphi)x_{H_2} \quad (20)$$

where $S_{l,CO}$ and S_{l,H_2} are the burning velocity of pure substances at the given equivalence ratio and the molar fraction x_i refers to the fuel mixture.

Conversely, in the presence of CO_2 , the trend of the laminar burning velocity is not linear, showing that at higher hydrogen content where the kinetic role of CO_2 is negligible, the trend is linear whereas at lower hydrogen content where the kinetic role of CO_2 is significant, the trend is not linear. In a previous paper Di Sarli & Di Benedetto (2007) have shown that the laminar burning velocity of $H_2/CH_4/air$ mixtures may be quite well correlated by means of the Le Chatelier-rule at lean and stoichiometric conditions.

In Figures 21-22 (bottom) the Le Chatelier (LC) correlation is shown as obtained for the $H_2/CO/O_2/N_2/CO_2$ mixtures according to the following:

$$S_l(\varphi) = \frac{1}{\frac{x_{CO}}{S_{l,CO}(\varphi)} + \frac{x_{H_2}}{S_{l,H_2}(\varphi)}} \quad (21)$$

From the results it can be concluded that the Le Chatelier rule does not fit the S_l data as a function of $H_2/(H_2+CO)$.

5.1.5. Anomalous behavior in syngas oxy-combustion explosions

The plots of Figures 15 - 17 show the typical story of deflagration combustion in closed vessel, with a maximum pressure (close to adiabatic pressure) and subsequent pressure decay due to heat losses towards vessel walls.

When enriching the syngas/O₂/N₂/CO₂ mixture with oxygen (Test 5), the pressure trend is qualitatively different (Figure 23).

The pressure history shows also a pressure peak (~ 200 bar), which over-takes the adiabatic pressure (6.9 bar). The occurrence of this anomalous behavior was previously found for CH₄/O₂/N₂/CO₂ mixtures and was named “combustion-induced Rapid Phase Transition” (c-RPT) [Di Benedetto et al., 2011].

It has been showed that the occurrence of this anomalous behavior is the result of the coupling of counter-acting phenomena: cycles of condensation and vaporization (at the vessel walls) of the water produced by combustion, which may culminate into a vapor explosion if the same water reaches the super-heating temperature (~ 450 K) [Reid, 1976; 1983].

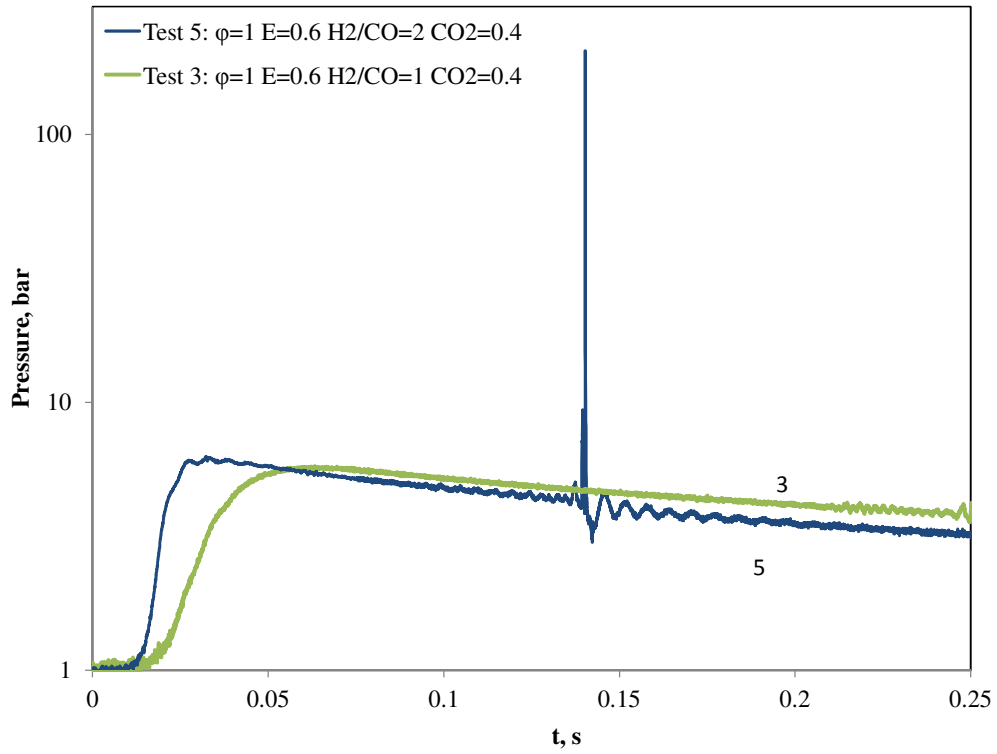


Figure 23. Pressure histories measured for Tests 3 and 5, with the evidence of c-RPT spikes. Composition blue line: 21.8% H_2 , 10.9% CO , 16.4% O_2 ; Composition green line: 16.4% H_2 , 16.4% CO , 16.4% O_2 .

5.2. Explosive behavior of H₂/CO/O₂/N₂ mixtures

The second part of activities has been devoted to the analysis of the explosion behavior of stoichiometric CO/H₂/O₂/N₂ mixtures, by varying either the oxygen enrichment factor from 0.21 (air) to 1 (pure oxygen), and the hydrogen to carbon monoxide ratio.

The main aim was to not observe the occurrence of the c-RPT in the absence of hydrogen, because no water can be formed from the combustion reaction. On the contrary, when introducing even small amount of hydrogen, the same phenomenon should occur if the thermodynamic and kinetic parameters for the c-RPT of the selected mixtures are satisfied.

The following Tables report the compositions of the mixtures investigated for different oxygen–air enrichment factors E in the absence of hydrogen (Table 6) and in the presence of hydrogen (Table 7), characterised by the hydrogen enrichment factors λ defined as in the following equation:

$$\lambda = \frac{H_2}{H_2 + CO} \quad (22)$$

In the same Tables, for each mixture the maximum theoretical values of pressure (P_{ad}) and temperature (T_{ad}), as computed by the Gaseq Chemical Equilibrium Program [GASEQ, 2011] in adiabatic conditions, and the corresponding molar composition of gaseous products are also reported. Finally, for the aims of discussion, Table 7 reports the partial pressure of the water produced by the combustion reaction (P_{H_2O}) as calculated at equilibrium conditions. It is worth noting that the water vapour pressure ($P_{H_2O}^0$) at the wall temperature ($T_{wall} = 283 \text{ K}$) is equal to 0.022 bar.

Table 6. Molar fractions of reactants and products, adiabatic temperature and adiabatic pressure for the tested mixtures as calculated at equilibrium conditions by GASEQ code.

E	Reactants			T _{ad} , K	P _{ad} , bar	Products				
	Y _{CO}	Y _{O2}	Y _{N2}			Y _{N2}	Y _{CO2}	Y _{CO}	Y _{O2}	Y _{NO}
0.21	0.296	0.148	0.556	2699.6	7.92	0.627	0.276	0.061	0.024	0.010
0.60	0.545	0.273	0.182	3201.8	9.03	0.204	0.387	0.257	0.106	0.023
0.80	0.615	0.308	0.077	3292.1	9.23	0.083	0.413	0.319	0.134	0.018
1.00	0.667	0.333	0.000	3360.0	9.40	-	0.428	0.371	0.157	-

Table 7. Composition of the reactive mixture, adiabatic temperature, adiabatic pressure, partial pressure of water and fuel conversion for the tested mixtures as calculated at equilibrium conditions by GASEQ code.

E	λ	Reagent mixture				T _{ad} , K	P _{ad} , bar	P _{H2O} , bar	X _{CO}	X _{H2}
		Y _{CO}	Y _{H2}	Y _{O2}	Y _{N2}					
0.21	0.010	29.3	0.3	14.8	55.6	2696.8	7.91	0.0199	70.9	99.7
0.21	0.101	26.6	3.0	14.8	55.6	2691.6	7.89	0.2397	73.6	97.0
0.30	0.011	37.1	0.4	18.8	43.8	2904	8.38	0.0232	63.2	99.6
0.30	0.040	36.0	1.5	18.8	43.8	2900.1	8.37	0.1089	64.3	98.5
0.35	0.010	40.8	0.4	20.6	38.2	2980.6	8.55	0.0211	59.5	99.6
0.40	0.009	44.0	0.4	22.2	33.3	3040.4	8.68	0.0193	56.3	99.6
0.40	0.040	42.7	1.8	22.2	33.3	3035.3	8.67	0.1243	57.6	98.2
0.45	0.011	46.9	0.5	23.7	28.9	3089.3	8.79	0.0240	53.5	99.5
0.45	0.040	45.5	1.9	23.7	28.9	3083.8	8.77	0.1279	54.9	98.1
0.50	0.010	49.5	0.5	25.0	25.0	3129.8	8.87	0.0224	50.9	99.5
0.55	0.010	51.9	0.5	26.2	21.4	3165	8.95	0.0211	48.5	99.5
0.60	0.009	54.0	0.5	27.3	18.2	3194.8	9.01	0.0199	46.4	99.5
0.60	0.101	49.1	5.5	27.3	18.2	3185	8.98	0.4094	51.3	94.6
0.80	0.010	60.9	0.6	30.8	7.7	3284.3	9.21	0.0216	39.5	99.4
0.80	0.020	60.3	1.2	30.8	7.7	3280.5	9.20	0.0576	40.1	98.9
1.00	0.010	66.0	0.7	33.3	0.0	3351.2	9.37	0.0234	34.5	99.3

Each composition was tested at least 2 times. For all tests, the initial pressure was set to 1 bar. The temperature of the vessel walls was equal to the ambient temperature (293 K).

5.2.1. Explosion of CO/O₂/N₂ mixtures: Effect of oxygen-air enrichment factor

In Figure 24, the pressure time histories are shown as obtained during explosions of CO/O₂/N₂ mixtures (hence no hydrogen) with oxygen-air enrichment factor varying from $E = 0.21$ (air) to $E = 1$ (pure oxygen). The plots are similar to typical pressure histories registered during closed vessel explosions, with small deviation between maximum pressure and adiabatic pressure (i.e., maximum theoretical pressure reported in the Figures 24 - - -), and pressure decay due to heat losses towards the external environment. The increase of E does not lead to a significant increase in maximum pressure (P_{\max}). On the other hand, the rate of pressure rise (i.e., the mixture reactivity) is clearly increased by the oxygen-enrichment.

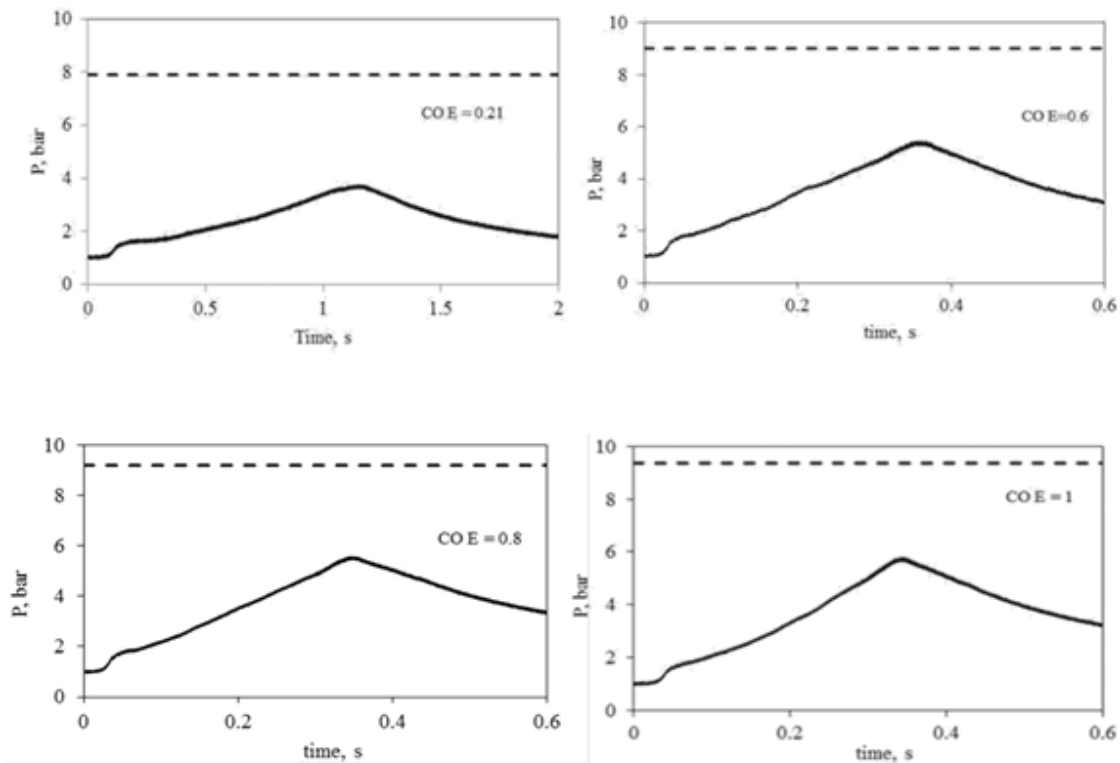


Figure 24. Pressure time histories as obtained during explosions of CO/O₂/N₂ mixtures with oxygen-air enrichment factor varying from $E = 0.21$ (air) to $E = 1$ (pure oxygen). The dotted line (- - -) represents the adiabatic pressure.

5.2.2. Effect of H₂ addition

Figure 25 shows the pressure time histories as obtained during explosions of CO/H₂/O₂/N₂ mixtures with different values of E and λ . In the presence of hydrogen, the pressure trends are qualitatively different from those shown in Figure 22. Indeed, the pressure histories for $E > 0.6$ exhibit a peak which over-takes the adiabatic value. This peak characterizes the above cited phenomenon of c-RPT.

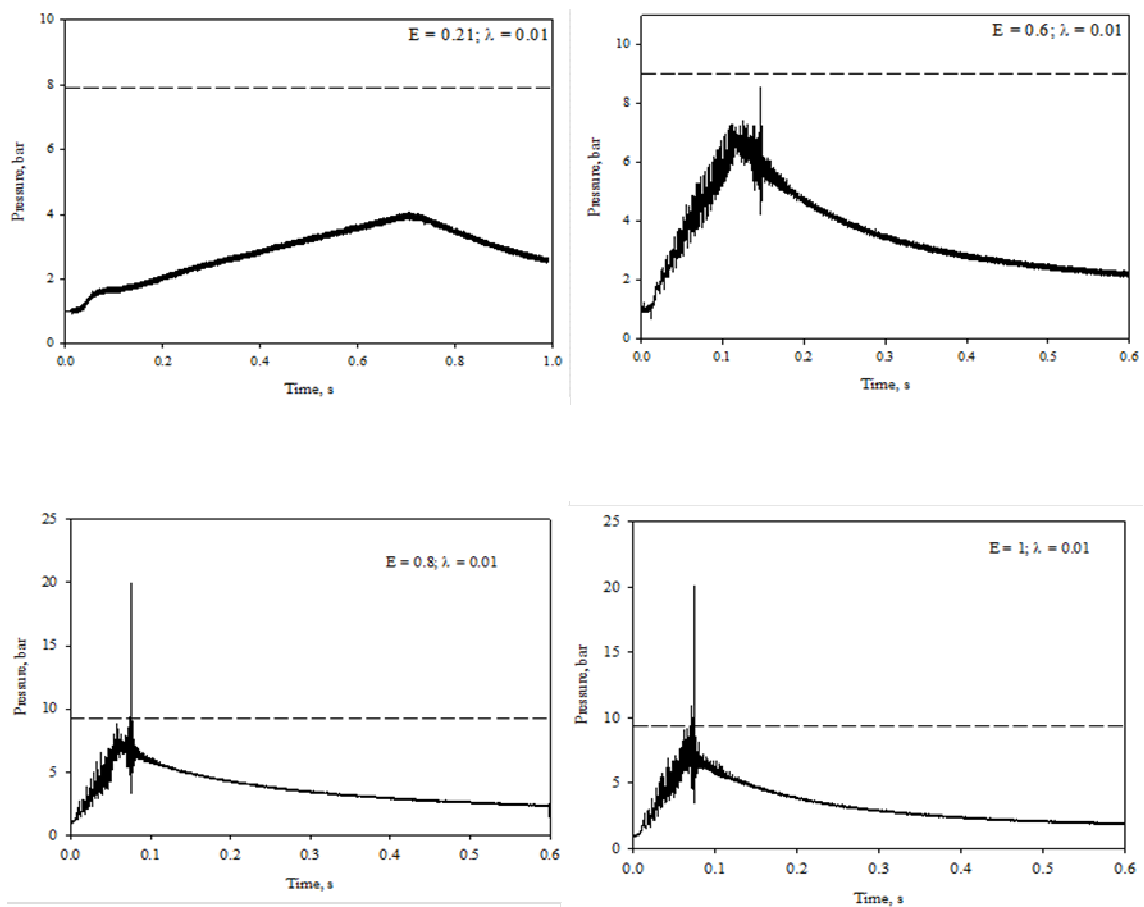


Figure 25. Pressure time histories as obtained during explosions of CO/H₂/O₂/N₂ mixtures with different values of E and λ . The dotted line (- -) represents the adiabatic pressure.

It is worth noting that pressure measurements have been realized through pressure transducer with natural frequency of 150 kHz and recorded by means of data acquisition system with frequency up to 1.0 MHz. That means c-RPT peak can not be considered a spurious point due to noise or electrical disturbance. Indeed the pressure history of the

spike is well described as shown in Figure 26 for the explosion of CO/H₂/O₂/N₂ mixtures with E=0.80 and λ=0.01, where the dots represent the actual experimental point as measured by the adopted pressure transducer..

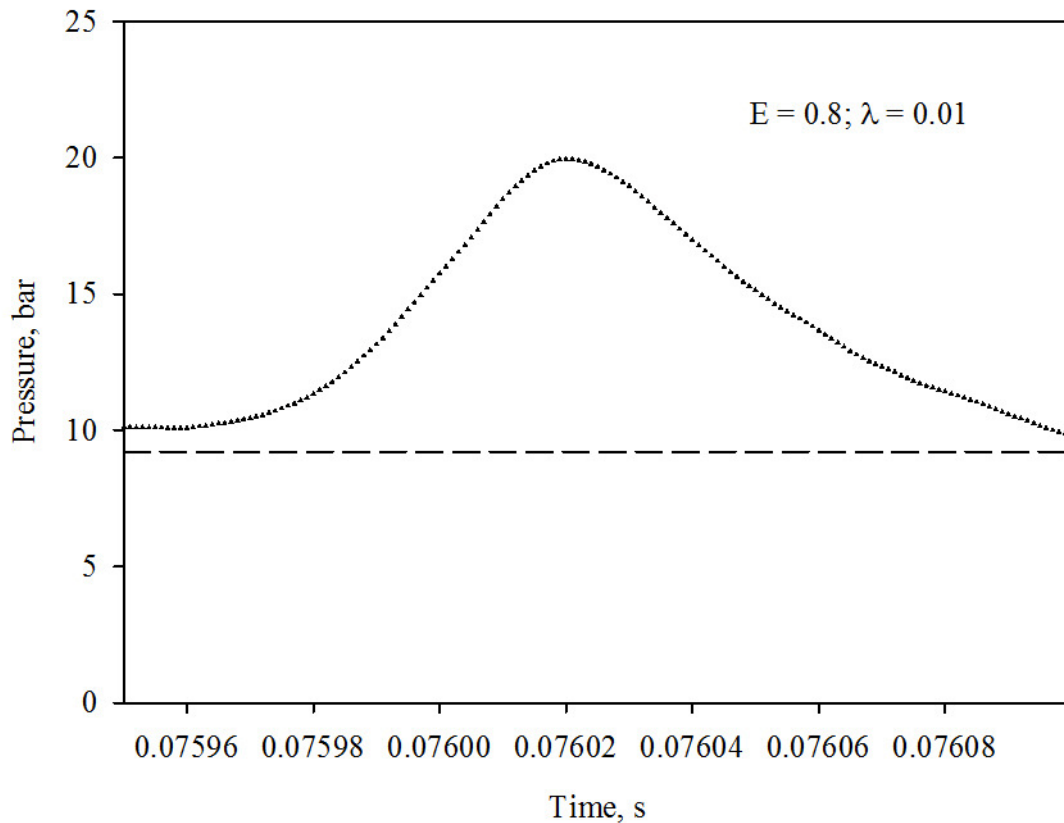


Figure 26. *c-RPT peak obtained CO/H₂/O₂/N₂ mixtures with E = 0.8 and λ= 0.01. The dotted line (- -) represents the adiabatic pressure. The dots are experimental points as measured by the adopted transducer.*

5.2.3. Enhancement of reactivity due to H₂ presence

Combustion kinetics is governed by the generation and propagation of radical species. In the case of CO combustion, reactions involving O radical and CO are very slow and, thus, it is extremely difficult to get ignition and flame propagation. When H₂ molecules or other species containing hydrogen (e.g., H₂O) are added to CO, the reaction rate considerably increases, because H radicals diffuse very rapidly enhancing chain branching reactions.

Table 8 reports the values of the maximum rate of pressure rise, $(dP/dt)_{\max}$, in the absence and presence of H_2 in the reactive mixture.

Table 8. *Adiabatic Temperature, T_{ad} , Adiabatic Pressure, P_{ad} , Rate of Pressure Rise in the early stage of reaction, dP/dt , Partial Pressure of Water, P_{H_2O} , Peak Pressure of c-RPT, P_{c-RPT} , for all compositions analyzed*

E	λ	T_{ad}, K	P_{ad}, bar	dP/dt, bar s⁻¹	P_{H_2O}, bar	P_{c-RPT}, bar
0.21	0	2699.6	7.92	24.5	-	-
0.60	0	3201.8	9.03	88.1	-	-
0.80	0	3292.1	9.23	81.2	-	-
1.00	0	3360.0	9.40	92.1	-	-
0.21	0.010	2696.8	7.91	53.3	0.0199	-
0.21	0.101	2691.6	7.89	206.6	0.2397	7.1
0.30	0.011	2904	8.38	105.4	0.0232	7.5
0.30	0.040	2900.1	8.37	175.1	0.1089	6.6
0.35	0.010	2980.6	8.55	151.9	0.0211	8.4
0.40	0.009	3040.4	8.68	192.5	0.0193	8.0
0.40	0.040	3035.3	8.67	297.0	0.1243	9.3
0.45	0.011	3089.3	8.79	224.1	0.0240	7.0
0.45	0.040	3083.8	8.77	399.1	0.1279	38.8
0.50	0.010	3129.8	8.87	330.4	0.0224	7.3
0.55	0.010	3165	8.95	322.6	0.0211	7.7
0.60	0.009	3194.8	9.01	413.2	0.0199	8.3
0.60	0.101	3185	8.98	2305.8	0.4094	337.8
0.80	0.010	3284.3	9.21	433.2	0.0216	15.4
0.80	0.020	3280.5	9.20	3961.0	0.0576	184.5
1.00	0.010	3351.2	9.37	868.0	0.0234	20.2

The rate of pressure rise increases with the oxygen (i.e., E factor) and hydrogen (i.e., λ factor) contents (Figure 27).

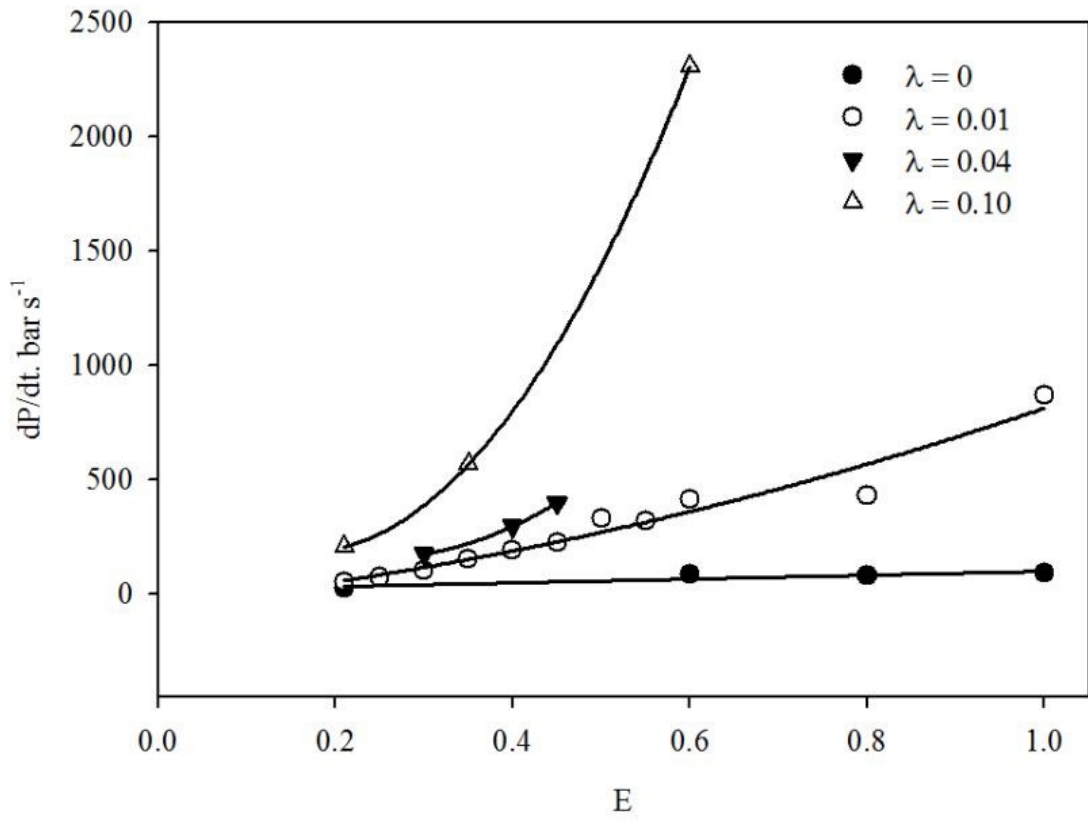


Figure 27. Rate of pressure rise versus E for different values of λ .

5.3. Theoretical prediction of c-RPT occurrence

The results obtained by the experimental tests reported previously have shown that the presence of H₂ induces intense pressure peaks due to the occurrence of c-RPT. In Table 8, the occurrence and intensity (peak pressure) of the c-RPT phenomenon are reported, together with the partial pressure of water in the given explosion conditions and the equilibrium data (adiabatic pressure and adiabatic temperature) for all mixtures investigated.

A first observation is that as λ increases the partial pressure of water in the gaseous products increases and the explosive phenomenon becomes more severe. Furthermore, even in the presence of small amounts of hydrogen, the c-RPT phenomenon is observed. That agrees with the explanation of the nature of c-RPT, which considers the partial pressure of water as the main parameter for the occurrence of the over-adiabatic spike. Indeed, for $\lambda = 0.01$, the value of the water partial pressure in the gaseous product ($P_{\text{H}_2\text{O}}$) is greater or about equal to the value of water vapor pressure ($P_{\text{H}_2\text{O}}^0$) at the wall temperature ($T_{\text{wall}} = 283 - 293 \text{ K}$; $P_{\text{H}_2\text{O}}^0 = 0.012 - 0.022 \text{ bar}$) and, thus, c-RPT may occur.

According to Lu et al. (1971), $\lambda = 0.01$ in H₂/CO/O₂ mixture (thus pure oxygen, E=1) is the limit value for triggering a deflagration to detonation transition. This means that, if the oxidizer is oxygen-enriched air (E < 1) $\lambda = 0.01$ in H₂/CO/O₂/N₂ mixture is a conservative choice to avoid detonation.

The occurrence and severity of the c-RPT phenomenon can also be explained through a theoretical analysis (Figure 28). In a closed vessel as that reported in the Figure, the flame propagates in both radial and axial directions. Due to heat exchange between bulk gas phase and cold walls of the reactor, the water produced by combustion reaction condense creating a liquid film on the vessel walls. The heat exchange between flame and wall/liquid

film through radiation determines an explosive evaporation of water if superheating temperature is reached.

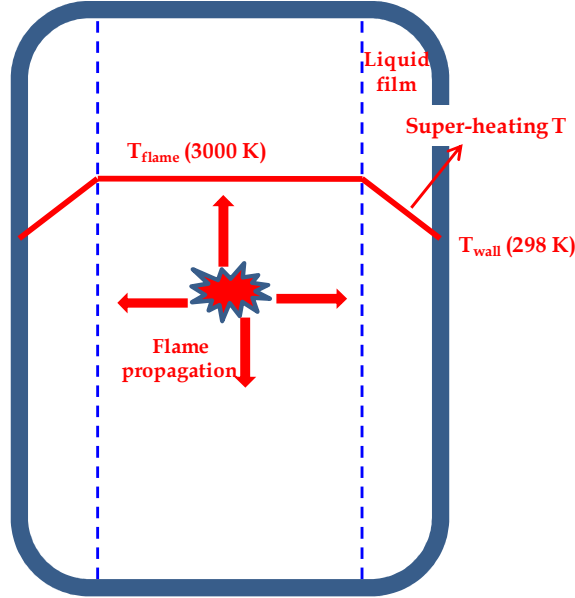


Figure 28. Schematic representation of the mechanism which trigger c-RPT

The c-RPT occurrence depends on the values of three characteristic times: τ_{reac} , τ_{cond} and τ_{rad} .

τ_{reac} is the time required by the flame to travel along the radial direction of the vessel.

$$\tau_{\text{reac}} = \frac{d}{2S_F} \quad (23)$$

where d is the reactor diameter and S_F the flame speed calculated as a function of the laminar burning velocity, S_l , and the expansion factor (i.e., the adiabatic pressure, P_{ad} , to initial pressure, P_o , ratio):

$$S_F = S_l \cdot \left(\frac{P_{\text{ad}}}{P_o} \right) \quad (24)$$

In Eq. 24, the expansion factor was evaluated assuming all gas as burned and at the maximum theoretical pressure (P_{ad}).

The term τ_{cond} is the time for water cooling and condensation at the vessel walls and is defined as:

$$\tau_{cond} = \frac{\rho c_p V}{h_c A} \quad (25)$$

where ρ and c_p are the density and the specific heat of the gas mixture; V and A are the volume and lateral surface of the vessel; h_c is the coefficient of heat transfer due to condensation at the walls evaluated according to the formula reported by Incropera & DeWitt (1996).

The term τ_{rad} is the time for heat exchange between flame and walls by radiation and was computed through the following formula:

$$\tau_{rad} = \frac{\rho c_p V (T_F - T_w)}{\sigma \epsilon A_R (T_F^4 - T_w^4)} \quad (26)$$

where T_F is the flame temperature (adiabatic temperature), σ the Stefan-Boltzmann constant, ϵ the emissivity and A_R the surface area enclosing the radiating gas volume.

Ultimately, the theoretical analysis needs the definition of two dimensionless factors:

$$\theta_1 = \frac{\tau_{cond}}{\tau_{reac}} \quad (27)$$

$$\theta_2 = \frac{\tau_{cond}}{\tau_{rad}} \quad (28)$$

In Table 9, the values of the characteristic times, the ratio between the condensation time and the reaction time ($\theta_1 = \tau_{\text{cond}}/\tau_{\text{reac}}$) and the ratio between the condensation time and the radiation time ($\theta_2 = \tau_{\text{cond}}/\tau_{\text{rad}}$) are given for the entire set of mixtures.

Table 9. Characteristic time of reaction, τ_{reac} , characteristic time of condensation, τ_{cond} , characteristic time of flame radiation, τ_{rad} , and dimensionless parameters θ_1 and θ_2 for all compositions analyzed

E	λ	$\tau_{\text{reac, S}}$	$\tau_{\text{cond, S}}$	$\tau_{\text{rad, S}}$	θ_1	θ_2	Notes
0.21	0	-	-	-	-	-	NO cRPT
0.60	0	-	-	-	-	-	NO cRPT
0.80	0	-	-	-	-	-	NO cRPT
1.00	0	-	-	-	-	-	NO cRPT
0.21	0.010	0.0180	0.0044	0.0032	0.25	1.38	NO cRPT
0.21	0.101	0.0076	0.0060	0.0191	0.78	0.31	under-adiabatic
0.30	0.011	0.0110	0.0047	0.0028	0.43	1.70	under-adiabatic
0.30	0.040	0.0066	0.0058	0.0100	0.88	0.58	under-adiabatic
0.35	0.010	0.0096	0.0045	0.0020	0.47	2.29	under-adiabatic
0.40	0.009	0.0086	0.0044	0.0015	0.51	3.00	under-adiabatic
0.40	0.040	0.0048	0.0059	0.0085	1.24	0.69	over-adiabatic
0.45	0.011	0.0072	0.0047	0.0019	0.66	2.52	under-adiabatic
0.45	0.040	0.0043	0.0058	0.0071	1.37	0.82	over-adiabatic
0.50	0.010	0.0067	0.0046	0.0015	0.69	3.05	under-adiabatic
0.55	0.010	0.0063	0.0045	0.0012	0.71	3.66	under-adiabatic
0.60	0.009	0.0061	0.0044	0.0010	0.73	4.32	under-adiabatic
0.60	0.101	0.0023	0.0060	0.0083	2.67	0.73	over-adiabatic
0.80	0.010	0.0049	0.0046	0.0009	0.94	4.95	over-adiabatic
0.80	0.020	0.0037	0.0055	0.0027	1.50	2.05	over-adiabatic
1.00	0.010	0.0041	0.0047	0.0009	1.13	5.38	over-adiabatic

Four different explosion behavior can be distinguished as function of the value assumed by

θ_1 :

- $\theta_1 \leq 0.2$, the explosion occurs in a deflagrative mode;
- $0.2 < \theta_1 < 1$, the pressure time history shows an oscillating behavior which not culminated into a peak over adiabatic. This behavior can be named “incipient c-RPT”;
- $\theta_1 \geq 1$ the pressure signal is oscillating and over-adiabatic behavior occurs. C-RPT behavior is found. Developed;
- $\theta_1 \gg 1$ a detonation mode is more likely.

These regimes are summarized and evidenced in Figure 29.

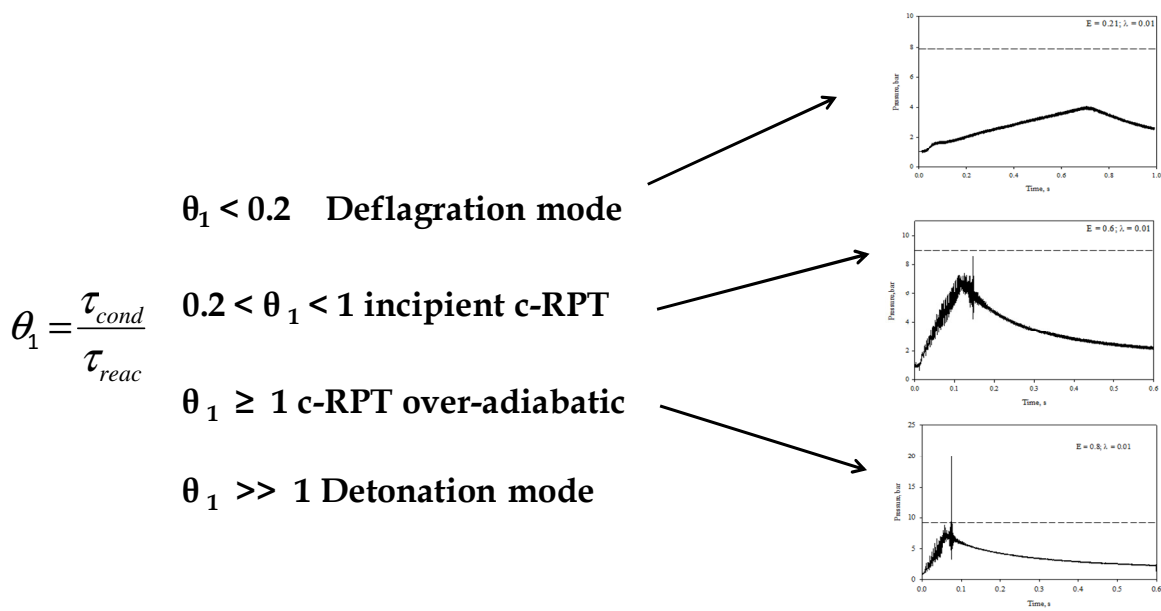


Figure 29. Criterion of occurrence and severity of c-RPT

It is worth noting that the value $\theta_1 = 1$ can be viewed as a bifurcation point. This result confirms the role of the synchronization between the reaction phase and the water condensation phase in driving the c-RPT phenomenon.

Figure 30 shows the map of the cRPT phenomenon with respect of oxygen enrichment factor (E) and hydrogen content (λ). The white zone of the map, characterized by $\lambda < 0.01$, was not investigated because of experimental limits in obtaining the mixtures. The circle size is proportional to θ_1 .

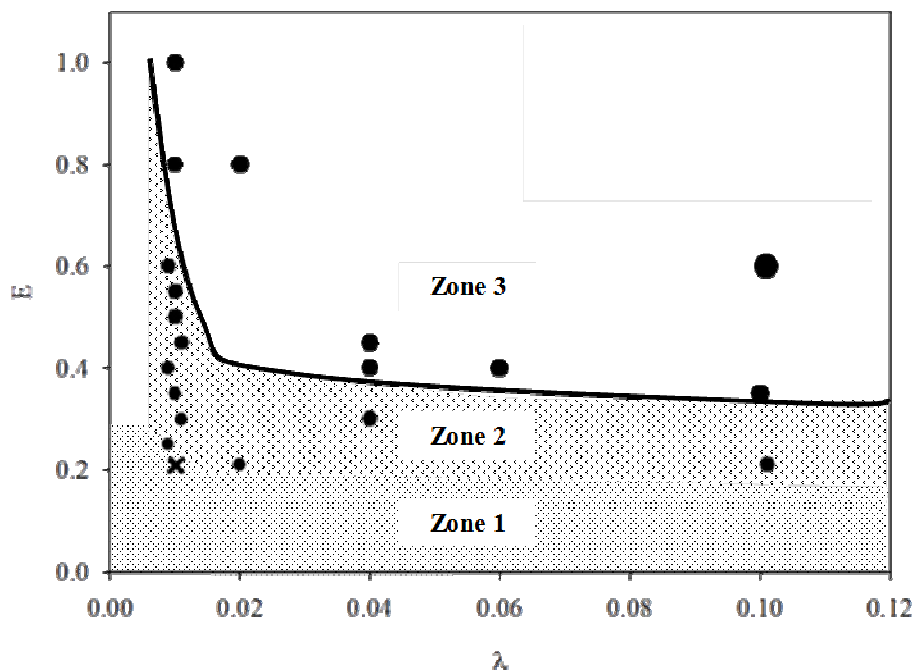


Figure 30. Occurrence and severity of c-RPT as function of E and λ .

Three zones may be distinguished:

- zone 1 - where no cRPT is found;
- zone 2 - where cRPT is found with peak pressure lower than the adiabatic value;
- zone 3 - where cRPT is found with over-adiabatic peak pressures.

In Figure 30 the dark line represents the limit between zones 2 and 3 and corresponds to the line $\theta_1 = 1$. It is worth noting that, for E higher than 0.4, the passage from zone 1 to

zones 2 and 3 occurs with increasing hydrogen content. It is also worth noting that a limit value of hydrogen content ($\lambda = 0.01$) is required for driving the c-RPT phenomenon, whatever the oxygen-air enrichment factor. In zones 2 and 3, as E and λ increase, the severity of the cRPT phenomenon increases and larger θ_1 values are found (and, thus, the circle size).

Figure 31 shows the same map in the plane of adiabatic temperature (T_{ad}) and water partial pressure (P_{H_2O}). In this case, however, the experimental results obtained by Di Benedetto et al. (2012) for $CH_4/O_2/N_2/CO_2$ mixtures are also reported with red circles, for the sake of comparison.

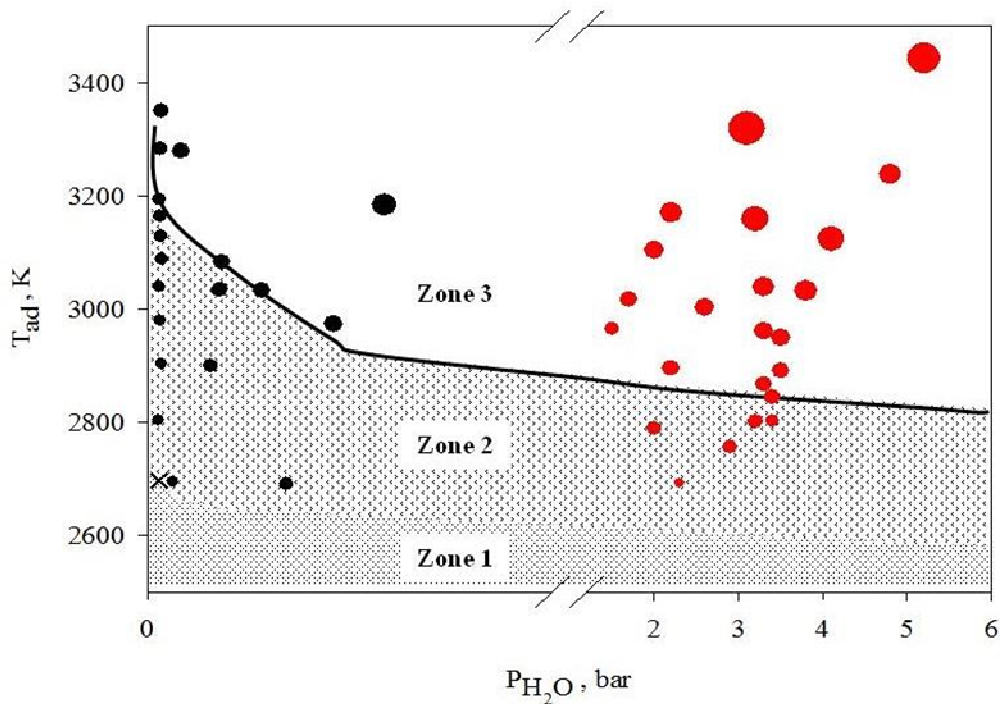


Figure 31. Occurrence of c-RPT as function of T_{ad} and P_{H_2O} . Black circles reproduce tests of this work, red circles represents experimental data obtained by Di Benedetto et al (2011)

In the plot, it is clearly demonstrated that if P_{H_2O} is lower than the water vapor pressure at the wall temperature or T_{ad} has low value, no c-RPT is found (zone 1). Furthermore, if P_{H_2O} is higher than the $P_{H_2O}^0$ value at T_{wall} , the c-RPT phenomenon occurs and the

maximum pressure can be under adiabatic (incipient c-RPT, zone 2) or over adiabatic (zone 3). Furthermore, it can be affirmed that the role of the adiabatic temperature in triggering c-RPT is also evident. Indeed, at a fixed value of the water partial pressure, the passage from zone 1 to zones 2 and 3 occurs with increasing adiabatic temperature. As the adiabatic temperature increases, the heating of the condensed water (by radiation) becomes faster, eventually synchronizing with the water condensation. As predicted by the θ_1 calculated values, also the red points are disposed on the map in the zones correspondent to their explosive behavior.

This map has a general validity and is independent by the nature of the fuel and the oxidizer. For this reason, it is possible to represent the results obtained for other mixtures if the values of T_{ad} and P_{H_2O} are known.

In Figure 32, θ_2 is plotted as a function of the adiabatic temperature, T_{ad} .

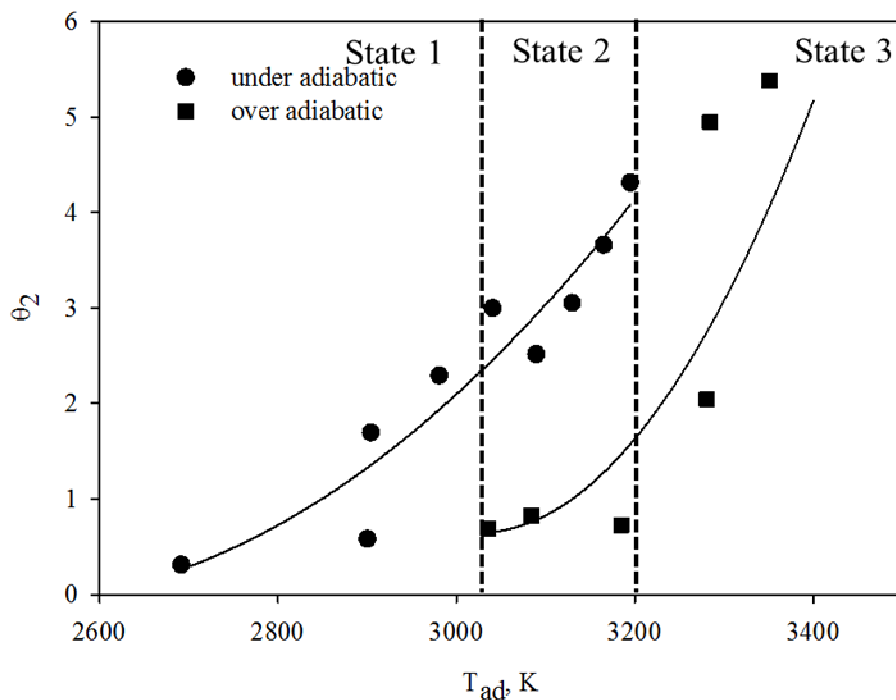


Figure 32. Characteristic time ratio θ_2 versus T_{ad} for under and over adiabatic behaviour of c-RPT.

Two main trends are identified: a low temperature zone and a high temperature zone. The low temperature zone corresponds to zone 2 of Figure 27, while the high temperature zone corresponds to zone 3. Three states are then identified.

- **State 1**, which lies at low temperature where only the incipient c-RPT behaviour is possible.
- **State 2**, in which both the incipient and over-adiabatic c-RPT behavior are possible. In this case, at the same flame temperature, the c-RPT is over-adiabatic when θ_2 is lower or close to 1, thus suggesting that the peak pressure overcomes the adiabatic values only if a strong synchronization between condensation and evaporation is established.
- **State 3**, at very high temperature ($T > 3200$ K), in which over-adiabatic c-RPT behavior is possible. In this case, the heating rate of the condensed water is very fast, thus driving the explosive boiling.

5.3.1. Analysis of literature data

The theoretical study conducted in the previous section can be easily applied to experimental results described in the open literature in order to explain the anomalous behavior often found in pressure history as c-RPT. In particular, experimental results obtained by BASF researcher (Safekinex, 2009) have been analyzed by calculating the dimensionless time ratio θ_1 (Table 10). For each composition, the dimensionless number θ_1 has been computed. It is clearly observed that at the conditions under which heat explosion is observed, it is $\theta_1 > 1$, thus suggesting that the c-RPT phenomenon has occurred. Conversely, during deflagration, θ_1 was found lower than 1. Detonation behavior has been found for θ_1 values bigger than 10^2 . In Figure 33 are reported white points corresponding to

the mixtures theoretically evaluated reported in Table 10, both for initial pressure of 1 bar and 5 bar.

Table 10: The occurrence of heat explosion as observed in SAFEKINEX project (Safekinx, 2009)

E = O₂/(O₂+N₂)	CH₄ %v/v	P₀ bar	P_{ad} bar	P_{max} bar	Explosion mode	θ₁
0.79	6.00	1.00	6.6	-	Deflagration	0.11
0.78	10.0	1.00	8.9	-	Heat explosion	1.14
0.75	20.0	1.00	12	-	Heat explosion	4.29
0.63	46.0	1.00	11	-	Deflagration	0.50
0.64	44.0	1.00	12	-	Deflagration	0.72
0.60	50.0	1.00	8.1	-	Deflagration	0.21
0.35	15.0	5.00	55	90	Heat explosion	30.5
0.67	25.0	5.00	68.5	140	Detonation	95.7
1.00	7.00	5.00	36.8	34	Deflagration	0.46
1.00	10.0	5.00	45.6	140	Heat explosion	3.41
1.00	12.0	5.00	50.1	210	Heat explosion	6.52
1.00	14.0	5.00	53.8	480	Heat explosion	9.98
1.00	15.0	5.00	55.5	505	Heat explosion	11.79
1.00	17.5	5.00	59.4	240	Heat explosion	16.42
1.00	20.0	5.00	62.9	470	Detonation	101.29
1.00	25.0	5.00	69.2	503	Detonation	133.29
1.00	35.0	5.00	80.1	310	Detonation	155.01
1.00	40.0	5.00	84	500	Detonation	135.34
1.00	45.0	5.00	85	920	Detonation	90.77
1.00	50.0	5.00	81.8	500	Detonation	51.84

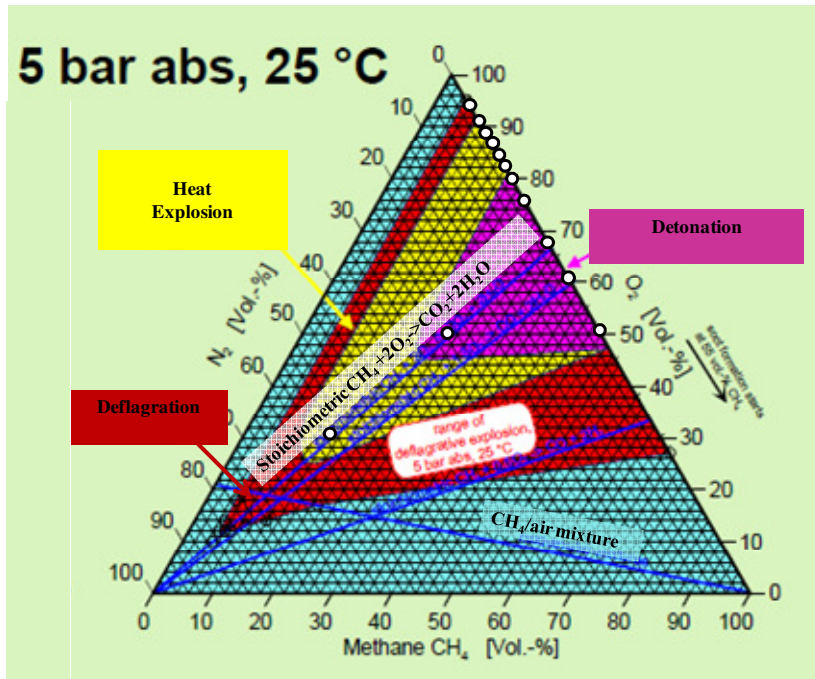
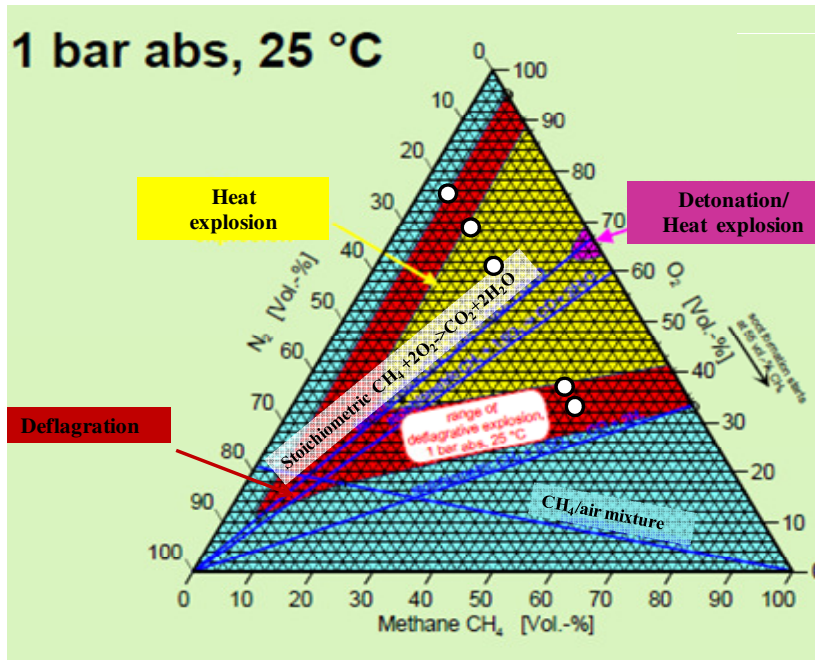


Figure 33. Triangular diagrams for $\text{CH}_4/\text{O}_2/\text{N}_2$ mixtures exploding in 20L sphere at initial pressure of 1 bar and 5 bar, [FP7 SAFEKINEX project, 2009]. White points represent the mixture theoretically analyzed for prediction of explosion mode.

6. CONCLUSIONS

The research activity conducted during my Ph.D. has been devoted to the evaluation of the effect of H₂/CO, oxygen-air enrichment, equivalence ratio and CO₂ content on the explosion behavior and reactivity of CO/H₂/O₂/N₂/CO₂ mixtures.

The activity has been realized by means of experimental tests and numerical simulations.

The nature of the CO₂ role in affecting the laminar burning velocity has been found to be mainly thermal at high values of the laminar burning velocity and both thermal and kinetic at low values of the laminar burning velocity.

The validity of additivity rules for burning velocity by varying the oxygen-enrichment factor, equivalence ratio, and CO₂ content has been verified. In particular, in absence of CO₂ the laminar burning velocity is a linear combination of H₂ and CO content, whatever the equivalence ratio and the oxygen content; conversely, in the presence of CO₂, the trend of the laminar burning velocity is not linear. Le Chatelier rule does not fit the SI data as function of H₂/(H₂+CO) in any case.

The experimental tests have showed the occurrence of an anomalous behavior for the pressure generation during explosion for highly oxygen enriched CO/H₂/O₂/N₂/CO₂ mixtures. In particular, it has been measured the presence of impulses with maximum overpressure up to 30 times the adiabatic pressure of combustion products in constant volume. Such phenomenon has been explained with the occurrence of a combustion-induced Rapid Phase Transition” (c-RPT), as reported in Di Benedetto et al. (2011) for the explosion of methane/oxygen-enriched air.

The explosive behaviour of CO/H₂/O₂/N₂ mixtures has been studied in a closed vessel by varying oxygen content (E), in the presence or absence of hydrogen in order to analyse the occurrence and the intensity of the c-RPT spike.

In the absence of hydrogen, as expected, either at stoichiometric condition in air or at any oxygen-enrichment factor and up to pure oxygen, the c-RPT phenomenon has not been observed. On the contrary, when adding even very small amount of hydrogen, the c-RPT phenomenon is excited and over-adiabatic peak pressures are reached. The obtained results confirm the key role of water in driving the c-RPT phenomenon.

A theoretical analysis based on the evaluation of characteristic time ratios of the explosive phenomenon has been conducted, in order to predict the occurrence and severity of c-RPT. When applying the criterion of the existence of the cRPT phenomenon to literature data, it turns out that they are the result of cRPT.

According to all these results, it can be affirmed that a new explosion mode has to be included in the general explosion classification which is due to the synergic coupling between a physical explosion (rapid phase transition) and a chemical explosion (deflagration), as shown in Figure 34.

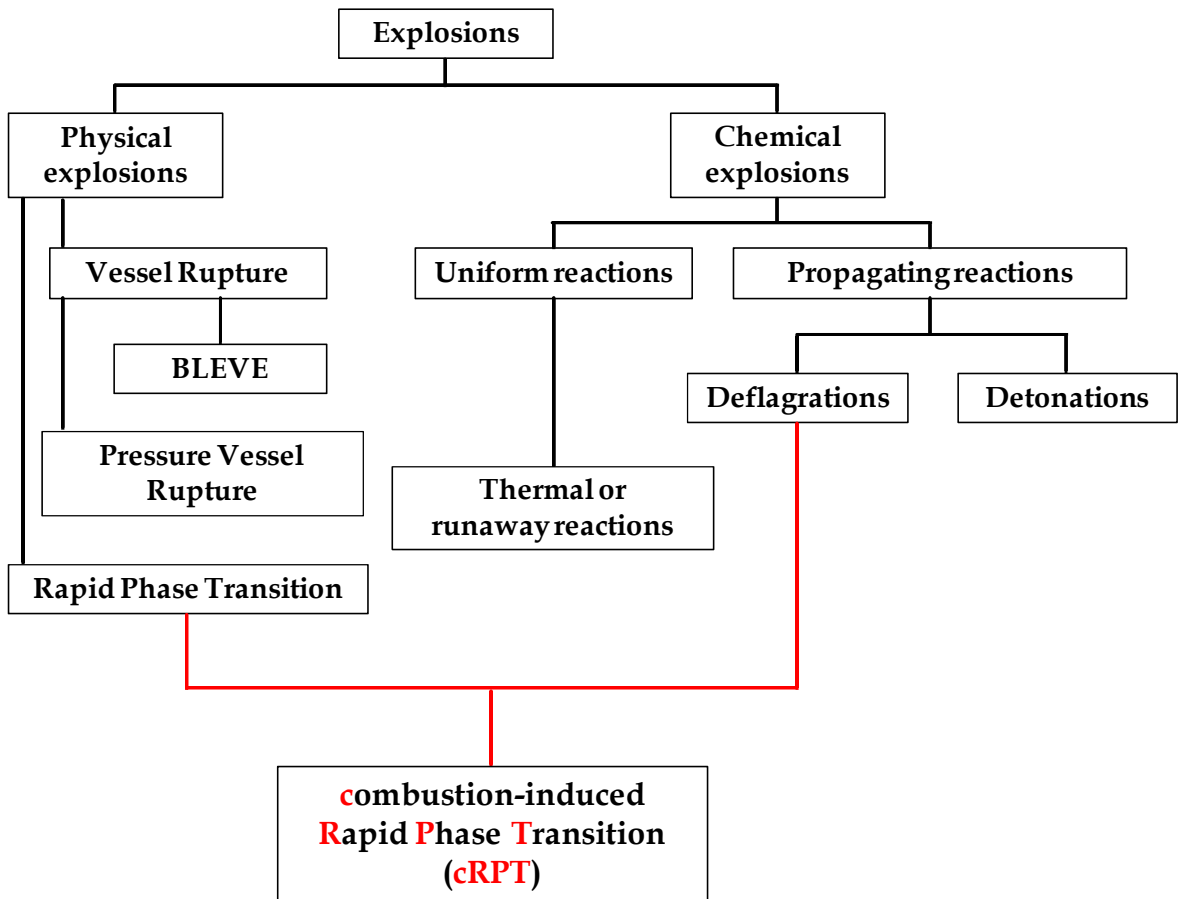


Figure 34: Explosion classification with the inclusion of the new explosion mode.

7. REFERENCES

- Akbar R., Kaneshige M.J., Schultz E., Shepherd J.E. *Detonations in H₂-N₂O-CH₄-NH₃-O₂-N₂ mixtures*. Technical Report FM97-3, Explosion Dynamics Laboratory, California Institute of Technology, **1997**.
- Arpenteiner, P.; Cavani, F.; Trifirò, F. *The Technology of Catalytic Oxidations. Safety Aspects.*; Ed. Technip: Paris. **2001**.
- Baulch, D.L., Drysdale, D.D., Duxbury, J., Grant, S., Evaluated kinetic data for high temperature reactions. **1973**, vol. 3, Butterworths, London.
- Bouvet, N.; Chauveau, C.; Gokalp, I.; Halter F. Experimental studies of the fundamental flame speeds of syngas (H₂/CO)/air mixtures. *Proc. Combust. Inst.* **2011**, 33, 913.
- Burke, M. P.; Qin, X.; Ju, Y.; Dryer, F. L. Measurements of hydrogen syngas flame speeds at elevated pressures. *5th US Combustion Meeting*. **2007**, 25.
- Chen, Z.; Qin, X.; Xu, B.; Ju Y.; Liu, F. Studies of radiation absorption on flame speed and flammability limit of CO₂ diluted methane flames at elevated pressures. *Proc. Combust. Inst.* **2007**; 31,2693.
- Crowl, D.A.; Louvar, J.F. *Chemical Process Safety, Fundamentals with Applications*, 2nd Ed., Prentice Hall, **2002**.
- Dahoe, A. E. Laminar burning velocities of hydrogen-air mixtures from closed vessel gas explosions. *J. Loss Prev. Process Ind.* **2005**, 18, 152.
- Dahoe, A. E.; De Goey, L. P. H. On the determination of the laminar burning velocity from closed vessel gas explosions. *J. Loss Prev. Process Ind.* **2003**, 16, 457.
- Davis, S. G.; Joshi, A. V.; Wang, H.; Egolfopoulos, F. An optimized kinetic model of H₂/CO combustion. *Proc. Combust. Inst.* **2005**, 30, 1283.

- Dennis, R. *The Gas Turbine Handbook*, National Energy Technology Laboratory, US Department of Energy, **2006**.
- Di Benedetto A., Cammarota F., Di Sarli V., Salzano E., Russo G., Anomalous behaviour during explosions of CH₄/O₂/N₂/CO₂ mixtures, *Combustion and Flame*, **2011**, 158, 2214.
- Di Benedetto A., Cammarota F., Di Sarli V., Salzano E., Russo G., Effect of diluents on Rapid Phase Transition of water induced by combustion, *AIChE Journal*, **2012a**, 58, 2810.
- Di Benedetto A., Cammarota F., Di Sarli V., Salzano E., Russo G., Reconsidering the flammability diagram for CH₄/O₂/N₂ and CH₄/O₂/CO₂ mixtures in light of combustion-induced Rapid Phase Transition, *Chemical Engineering Science*, **2012b**, 84, 142.
- Di Benedetto A., Cammarota F., Di Sarli V., Salzano E., Russo G., Combustion-Induced Rapid-Phase Transition (cRPT) in CH₄/CO₂/O₂-Enriched Mixtures, *Energy&Fuels*, **2012c**, 26, 4799.
- Di Benedetto A., Di Sarli V., Salzano E., Cammarota F., Russo G., Explosion behavior of CH₄/O₂/N₂/CO₂ and H₂/O₂/N₂/CO₂ mixtures. *Int. J. Hydrogen Energy*. **2009**, 34, 6970.
- Di Sarli, V.; Di Benedetto, A. Laminar burning velocity of hydrogen–methane/air premixed flames. *Int. J. Hydrogen Energy*. **2007**, 32, 637.
- Ding, N.; Arora, R.; Norconk, M.; Lee, S. Y. Numerical investigation of diluent influence on flame extinction limits and emission characteristic of lean-premixed H₂/CO (syngas) flames. *Int. J. Hydrogen Energy*. **2011**, 36, 3222.
- Dupré G., Peraldi O., Joannon J., Lee J.H., Knustautas R., AIAA, Prog. Astronaut., Aeronaut., **1990**, 133,156.

GASEQ, A Chemical Equilibrium Program for Windows. Available at:
<http://www.c.morley.dsl.pipex.com/>.

Glassman, I., Yetter, R.A., *Combustion*, Fourth Edition, **2008**, Academic Press

H.J. Michels, G.Munday and A.R.Ubbelohde, Detonation Limits in Mixtures of Oxygen and Homologous Hydrocarbons, *Proc. R. Soc. Lond. A.*, **1970**, 319, 461.

Hassan M.I., Aung K.T., Faeth G.M., *J. Propul. Power*. **1997**, 13, 239.

Hendershot R.J., Lebrecht T.D., Easterbrook N.C., Use oxygen to improve combustion and oxidation, *AIChE Journal*, **2010**.

Huang, Z.; Zhang, Y.; Zeng, K.; Liu, B.; Wang, Q.; Jiang, D. Measurements of laminar burning velocities for natural gas-hydrogen-air mixtures. *Combust. Flame*. **2006**, 146, 302.

Incropera, F. P.; DeWitt, D. P. *Fundamentals of Heat and Mass Transfer*, 4th Ed, John Wiley & Sons Inc.: New York, **1996**.

Kee, R. J.; Grcar, J. F.; Smooke, M. D.; Miller, J. A. A FORTRAN program for modeling steady laminar one-dimensional premixed flames. Sandia National Laboratories Report, SAND **1985**, 85,8240.

Kim, C. H.; Kwon, O. C.; Faeth, G. M. Effects of halons and halon replacements on hydrogen-fueled laminar premixed flames. *J. Propul. Power* **2002**,18, 1059.

Law, C. K.; Kwon, O. C. Effects of hydrocarbon substitution on atmospheric hydrogen–air flame propagation. *Int J Hydrogen Energy*, **2004**, 29, 867.

Lee, J.H.S. *The detonation phenomenon*, Cambridge University Press: New York, **2008**.

Lewis, B.; Von Elbe, G. *Combustion, flames and explosions of gases*, II Ed. Academic Press: New York, **1961**.

- Li J., Kazakov A., Zhao Z., Chaos M., Dryer F.L., Scire J.J., A comprehensive kinetic mechanism for CO, CH₂O, and CH₃OH. *Int. J. Chemical Kinetics*. **2007**, 39, 109.
- Lieuwen, T. C.; Yang, V.; Yetter, R.; *Synthesis Gas Combustion: Fundamentals and Applications*, CRC Press, Taylor & Francis, **2010**.
- Lu, P.L., Dabora, E.K., Nicholls, J.A., The role of explosion limit chemical kinetics in H₂-CO-O₂ detonations, *Combust. Flame*, **1971**, 16, 195.
- McLean I.C., Smith D.B., Taylor S.C., The use of carbon monoxide/hydrogen burning velocities to examine the rate of the CO + OH reaction. *Proc. Combust. Inst.* **1994**, 25, 749.
- Mittal G., Sung C.J., Fairweather M., Tomlin A.S., Griffiths J.F., Hughes K.J., Significance of the HO₂ + CO reaction during the combustion of CO + H₂ mixtures at high pressures. *Proc. Combust. Inst.* **2007**, 31, 419.
- Moen I.O., Murray S.B., Bjerkedvedt D., Rinnan A., Knystautas R., Lee J.H.S., Nineteenth Symposium (International) on Combustion, Combustion Institute, Pittsburgh, **1982**, 5635.
- Natarajan, J.; Lieuwen, T.; Seitzman, J. Laminar flame speeds of H₂/CO mixtures: Effect of CO₂ dilution, preheat temperature, and pressure. *Combust. Flame*. **2007**, 151, 104.
- Petersen E.L., Kalitan D.M., Barrett A.B., Reehal S.C., Mertens J.D., Beerer D.J., Hack R.L., McDonnell V.G., New syngas/air ignition data at lower temperature and elevated pressure and comparison to current kinetics models. *Combust. Flame*. **2007**, 149, 244.
- Prathap, C., Ray, A.; Ravi, M. R. Investigation of nitrogen dilution effects on the laminar burning velocity and flame stability of syngas fuel at atmospheric condition. *Combust. Flame*. **2008**, 155, 145.

- Reid, R. C. Rapid phase transitions from liquid to vapor. *Advances in Chemical Engineering*. **1983**, 12, 105.
- Reid, R. C. Superheated liquids. *American Scientists*. **1976**, 64, 146.
- Richards, G. A.; Casleton, K.H.; Chorpening, B.T. CO₂ and H₂O Diluted Oxy-Fuel Combustion for Zero-Emission Power. *Int. J. Power Energy*. **2005**, 219, 121.
- Safekinx, SAFe and Efficient hydrocarbon oxidation processes by KINetics and Explosion eXpertise, "Energy, Environment and Sustainable Development" Programme (Contract Number EVG1-CT-2001-00098), **2009**.
- Salzano, E., Cammarota, F., Di Benedetto, A., Di Sarli, V., Russo G. Combustion-Induced Rapid Phase Transition of CH₄/O₂/Inert Mixtures, *Chemical Engineering Transactions*, **2013**, 31, 883.
- Savitzky K., Golay M. J. E., Smoothing and Differentiation of Data by Simplified Least Squares Procedures, *Analytical Chemistry*, **1964**, 36, 1627.
- Sun, H.; Yang, S. I.; Jomaas, G.; Law, C. K. High-pressure laminar flame speeds and kinetic modeling of carbon monoxide/hydrogen combustion. *Proc. Combust. Inst.* **2007**, 31, 439.
- Tang, C.; Huang, Z.; Wang, J.; Zheng, J. Effects of hydrogen addition on cellular instabilities of the spherically expanding propane flames. *Int. J. Hydrogen Energy*. **2009**; 34, 2483.
- Thomas, G.O., Flame acceleration and the development of detonation in fuel–oxygen mixtures at elevated temperatures and pressures, *J. Hazardous Materials*. **2009**, 163, 783.

- Uykur, C.; Henshaw, P. F.; Ting, D. S-K.; Barron, R. M. Effects of addition of electrolysis product on methane/air premixed laminar combustion. *Int. J. Hydrogen Energy*. **2001**, 26, 265.
- Van Maaren, A.; Thung, D. S.; De Goey, L. P. H. Measurement of flame temperature and adiabatic burning velocity of methane/air mixtures. *Comb Sci Technol*. **1994**, 96, 327.
- Walton, S. M.; He, X.; Zigler, B. T.; Wooldridge, M. S. An experimental investigation of the ignition properties of hydrogen and carbon monoxide mixtures for syngas turbine applications. *Proc. Combust. Inst.* **2007**, 31, 3147.
- Warnatz, J., Maas, U., Dibble, R.W., *Combustion*, 4th Edition, **2006**, Springer.
- Yetter, R. A.; Dryer, F. L.; Rabitz, H. A comprehensive reaction mechanism for carbon monoxide/hydrogen/oxygen kinetics. *Comb Sci Technol*. **1991**, 79, 97.